Plane-Strain Fracture Toughness and Tensile Testing of a Piezoelectric Composite for Spinal Fusion

By

Kelly Tong

Submitted to the graduate degree program in Bioengineering and the Graduate Faculty of the University of Kansas in partial fulfillment of the requirements for the degree of Master of Science

_____

Chairperson Dr. Elizabeth Friis

_____

Dr. Sara Wilson

_____

Dr. Carl Luchies

Date Defended: December 12th, 2017

The Thesis Committee for Kelly Tong

certifies that this is the approved version of the following thesis:

Plane-Strain Fracture Toughness and Tensile Testing of a Piezoelectric Composite for Spinal Fusion

_____

Chairperson Dr. Elizabeth Friis

Date Approved: January 29th, 2018

Abstract

A novel piezoelectric spinal fusion device has been shown to improve spinal fusion. The mechanical properties of this novel piezoelectric material are important for the integrity of the device. To characterize the mechanical properties of the piezoelectric material, a uniaxial tensile test and a plane-strain fracture toughness test used to determine the mechanical integrity of the material. The specific materials investigated were a pure layered stack made of piezoelectric discs and piezoelectric discs stacked with intermediate compliant layers. Results of tensile testing were inconclusive. Stress concentrations around the layers and the brittle nature of the material caused early failure. Results of fracture toughness were unreliable due to a flaw in the experimental procedure. Theoretical calculations were performed to determine the potential fracture toughness of the material, resulting in a higher fracture toughness for the piezoelectric discs stacked with intermediate compliant layers as compared to the pure layered piezoelectric discs. Additional fracture toughness testing yielded preliminary fracture toughness values. A single sample with compliant layers had a higher fracture toughness than a single sample without the compliant layers. However, additional work with a larger sample size needs to be performed to determine statistical significance.

Acknowledgements

Mother and Sister: I want to thank you both for always being the supporters who pushed me to be a better version of myself. Jeanne, you are the voice in my head that keeps me going by reminding me to be determined and work hard. You two are the strongest women I have and will ever know in my life. Both of you inspire me to always strive to be the best. I am grateful Mom that you gave me and Jeanne a chance by being the strongest, most humble, and caring single mother I could ask for. I would not be where I am today without you fighting for me and providing everything you can as a single mother. Thank you so much mom, I love you so much. Jeanne, I want to thank you for always supporting me even when I don't agree with mom's opinions or vice versa. You have always been there to comfort me when I am at my lowest. You're the best friend and best sister I could ever have.

Grandmother: Although you won't be able to read this because it isn't translated. I just want to thank you as well for always believing in what I do no matter what, even when no one would agree. You have raised me to be who I am today. You always come in first when it comes to spending time at home because you always know how to keep me fed especially when I am stressed.

Aaron Butler: Thank you for being the rock of it all. You've held me together when things don't go as planned. Thank you especially for always taking care of me and constantly doing everything for me when I am so stressed, that I cannot even sleep or relax. I know I can always count on you to make me laugh through the hardest times.

Most of all, thank you for believing in me in whatever I strive to do. I love you with all of my heart.

Melissa: I just want to give a huge thanks to my soul sister for always checking on me to make sure I still am myself. Thank you for being by my side no matter what and most of all thank you for that shamrock shake 6 years ago.

Dr. Lisa Friis: Thank you for being one of the wisest adviser's I have met, as well as being a mentor for life. Without you I would not have had such a great opportunity to have experienced what I have at KU compared to others who are in my place. No other lab that I would have applied for at a different university could have given the industry experience and real-world application that the spine lab has. Your passion and drive as a professor and a colleague inspires me as a woman in engineering. I cannot thank you enough for always challenging me and providing the support when I need it. Most of all I cannot thank you enough for all your time that you have put aside to make sure that I have what it takes to succeed.

Dr. Luchies: Thank you for being a wonderful professor and welcoming me with such a great experience in your ADAM's class. The mechanical engineering experience I had in your class, being a first-year master student, with a biomedical background, will remain with me always. Your type of class and the skills I gained from it is one of the many things here at KU that have cemented my original decision to come to graduate school. I also want to thank you for taking the time to be a part of my committee, your time and effort is greatly appreciated.

Dr. Wilson: Thank you for teaching me all the lessons of ethics and helping my product development team thrive. The life lessons you've shared with me will always be in the back of my mind. I will miss being able to spend "working hours" at a coffee shop and learning how to deal with difficult situations. These lessons will surely be brought with me at my future job, and I know now that I will be handle ethical dilemmas when they come up. Thank you too for taking the time to be a part of my committee!

Kyle Coates: Thank you for being my partner in crime in our lab. Your kindness never ends and reminds me that humanity isn't all too bad. You're always willing to help, be there when I rant my brains off, and most of all be there to be the calm to my frustration. Thank you for being the one of the best lab mates ever.

Eileen: Thank you for always being the older sister I never had, and always wanting the best for me. You have helped me so much in viewing things in a better light than I normally would. I also want to thank you for giving me wise advice and always playing devil's advocate, and most of all helping me throughout all my work in the lab with brainstorming to general life advice. Thank you, Eileen!!

Ember: Thank you for always constantly being the mom of the lab by making me check and double check things. Without you, I'd probably lose my head. Thank you for also adding some sass and margaritas into my life. I can never have enough of that! You are one of the most reliable, and caring individuals I have ever known. I know I can always count on you to have a doggie date. Most of all thank you for keeping me sane throughout all my work in the lab by reminiscing about our love of Denmark and NM. I couldn't be more grateful for the help you have provided me at my time here at KU. Thank you.

Alyssa: Thank you so much for reeling me into KU! I would have never had such an experience without you. I am so thankful I made that phone call to you a few years ago. You encouraged me and gave me the confidence that I too could tackle graduate school. I am so thankful to have met someone who dedicated so much time into preparing me for acceptance day, making me feel at home when I got here, and most of all being the Bucknell Alum I could count on. Thank you so much Alyssa!

Table of Contents

Figures List

Tables List

Chapter 1: Background and Significance

1.1 Introduction

To understand the purpose of this work, background knowledge regarding spinal fusions, piezoelectric materials, mechanical testing, and general composite theory is necessary. The first few sections of this chapter will discuss the overarching goal, while the background knowledge necessary to perform this work will follow in subsequent sections.

Characterization of materials is important for designing an implant. Biocompatibility and mechanical properties are two components of characterizing a novel material. This is especially important in the realm of spinal fusions. Understanding the mechanical properties insures that a material selected for spinal fusion devices does not fail. The material must also withstand the compressive loading produced by the anterior structures of the spine, maintain height in between vertebrae, and allow for fusion to take place to provide stability.[1],[2] [3]The strength and the fracture toughness (crack propagation resistance) are properties important in determining an appropriate material to be used in spinal fusion devices. This study will investigate two novel composite materials developed for a spinal fusion implant.

1.2 Spinal Fusion

1.2.1 General Spinal Fusion and Interbody Devices

Standard treatment available for degenerative spine diseases is spinal fusion due to its effectiveness.[4],[5] The annual volume of increase in spinal fusions is 137%.[4] During a spinal fusion procedure, the degenerative component or the severely degenerated disc in between two vertebrae, is removed (Figure1).

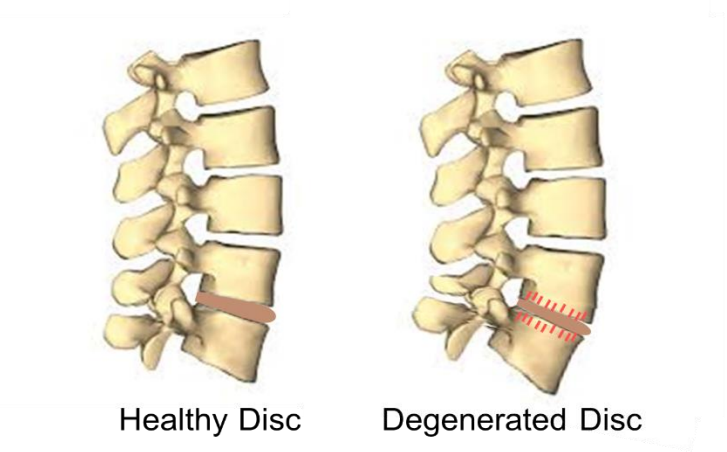

Figure 1: Image of a degenerated disc that would be removed during spinal fusion surgery. Also in comparison is what a healthy disc should look like, clearly supporting the two vertebrae above and below. The red on the unhealthy disc represents the beginning damage of the vertebrae. (Public Domain, modified for use)

Spinal fusion surgery is performed over 250,000 times a year in the United States alone.[6] After removal of the vertebral disc, an interbody device helps the two vertebrae fuse together. An interbody device is known as an interbody cage, and it is placed in the intervertebral space to help transmit the load through the spine while screws and rods provide stability to the vertebrae as the fusion site heals (Figure 2). Once the vertebrae are stabilized, the interbody can aid in transmitting load from one

vertebral body to the next. Surgeons will also place a bone graft along with the interbody cage to help guide bone cells into growing in between the two vertebrae, thus allowing for fusion. There may be loss of motion after full fusion, however, the patient regains stabilization and reduction in pain due to the ability of the spine to transmit loading properly again through the vertebrae.[7],[8]

Figure 2: Image of a degenerated disc removed and replaced with interbody device during spinal fusion surgery. (Public Domain, modified for use)

Unsuccessful fusion however, may lead to second surgeries and additional discomfort for the patient. Patients with good health are not unsusceptible to non-fusion, as there is still a 20 to 40% chance of failure.[9] Additionally patients with risk factors such as tobacco users and diabetics, often only have a fusion rate of 70% and 80%;

whereas patients without such risk factors exhibit 90% or higher fusion within the first two years of having the surgery.[9],[10] These patients often cannot be elected for the procedure because their preoperative conditions (tobacco users, diabetics, obesity) put them at risk of non-fusion.[11]–[13] Although the risk factors decrease a patient's ability to fuse, there is a possibility for these patients to still undergo spinal fusion with the use of direct current electrical stimulation.[14] A study done by Rogozinski, found 96% of patient population within the study, which included smokers, did have successful fusion using direct current stimulation in comparison to those who did not have stimulation.[15]

1.2.2 Mechanism of Electrical Stimulation of Bone & Current Devices

It has been widely shown that electrical stimulation has been highly effective in bone recovery.[9] Bone recovery was originally described in Wolff's Law describing the concept that applied stress to bone can cause bone formation (Figure 3).[16] This law was further developed by Yasuda who discovered that bone in tension was electropositive, while bone in compression was electronegative.[16] Yasuda ultimately discovered that there is a piezoelectric effect in bone.[17] His discovery led to more investigations revealing the bone's response to electrical stimulation because of this effect, however, the true nature of the biological mechanism is still not clear.[18] However, there have been studies performed showing possible mechanisms to bone formation depending on the types of electrical stimulation such as direct current stimulation or capacitive coupling stimulation.[19],[20]

With DC (direct current) stimulation, during experimentation it was observed that the osteoinductive factors (bone's normal regulators during bone production) are upregulated due to gene expression that controls these factors.[14], [21]–[23] Therefore,

when electrical stimulation is applied to a certain location of the bone, growth factors increase. The increase in growth factors can promote fusion of a non-union in bone, specifically bone similar to a growth plate (active bone), and resulting bone formation on a bone graft improves.[14], [24] Understanding possible mechanisms provides possible explanation to the efficacy of future electrical stimulation devices, as well as, those that have been recently successful.

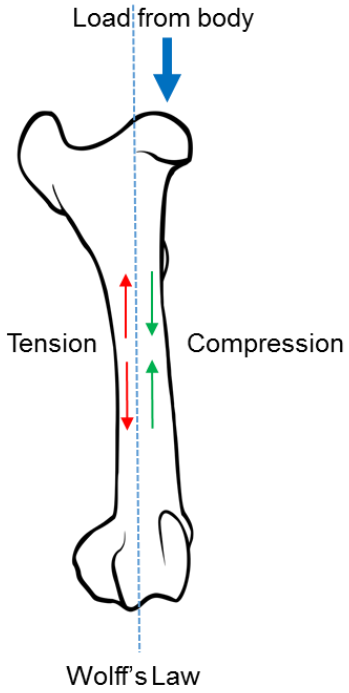

Figure 3: Schematic of mechanotransduction in bone, and how remodeling of bone/healing occurs. This exhibits Wolff's Law and the dynamic loading of compression and tension causes an electrical potential thus stimulating bone growth with this applied force (Public Domain).

The direct current bone healing solutions that currently exist usually require an addition of a battery-operated component external to the implantation of the device. This device has been studied as early as 1988 when Kane used a DC stimulation device in posterior spinal fusions performed clinically and was able to achieve 81% success of fusion compared to only 54% success of those without the device.[25] Further

experimentation by Tejano, produced results in which patients recruited had a 92% success rate with even multiple-level (multiple vertebrae needing to be fused) spinal fusions.[26] Although successful in fusion, the battery-operated alternative to a spinal fusion interbody is not desirable as it is a Class III device, and thus comes with higher risk to the patient. Additionally, users are noncompliant to wearing the stimulation device and thereby eliciting it less effective than intended.[27] Therefore, it is ideal to use an internal source to stimulate bone healing. However, the internal technology available to stimulate bone requires a battery pack implanted along with the cage to provide the DC stimulation necessary to promote bone growth, such as the Bagby and Kuslich (BAK) cage (Figure 4), among many others.[9] The Bagby and Kuslick cage has also only been used a sheep study, and has yet to be used in humans. Although such devices have shown higher fusion rates compared to traditional methods, in sheep, there are still shortcomings of using such cages.

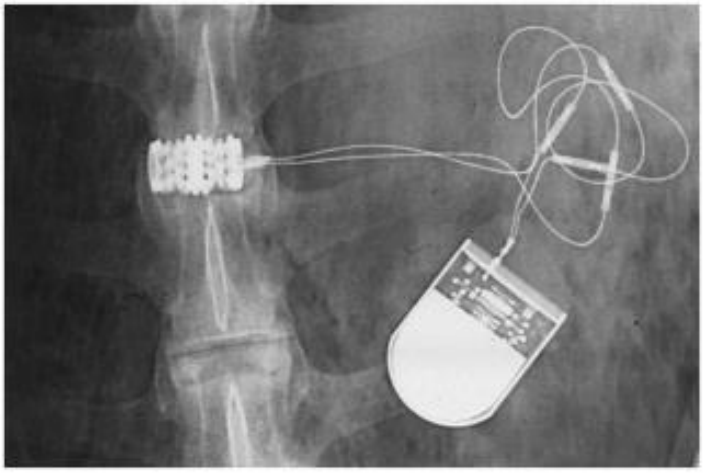

Figure 4: Plane anteroposterior radiograph of the laterally placed Bagby and Kuslich (BAK) cage in the ovine L4-L5 level with leads extending to the subcutaneously placed direct current stimulator. In the 0-[mu]A current group, no device was attached to the leads. Image of a BAK cage with its battery pack implanted in sheep to demonstrate fusion from DC stimulation. It is clear the battery is a separate component that is attached to the electrodes (With Permission). [9]

Such cages are designed to supply constant current to the affected area, a battery pack or power source is necessary internally, and electrodes/leads along with the battery pack need to be placed into the soft tissue near the healing site, invasively.[28],[29] Constant supply of current to the affected area is not ideal because once full fusion takes place, the device has no method of disabling itself, and can continue potentially longer than the necessary 6 to 9 months.[16] Additionally, a battery pack or power source contains a battery that needs to be eventually removed, which introduces a second invasive surgery for the patient.[16],[30] Current DC stimulation devices also requires the electrodes and the battery pack, to be placed directly near the healing site, which can introduce longer time for spinal fusion surgery again posing risk to the patient from an anesthetic point of view.[16] For the reasons aforementioned, electrical stimulation of bone has high potential, but there is still a need for an improved *in vivo* device that delivers electrical stimulation.

1.3 Piezoelectric Material

A piezoelectric (PZT) material is a material in which mechanical loading or stresses applied results in production of voltage as the response (Figure 5).[31] Because of this

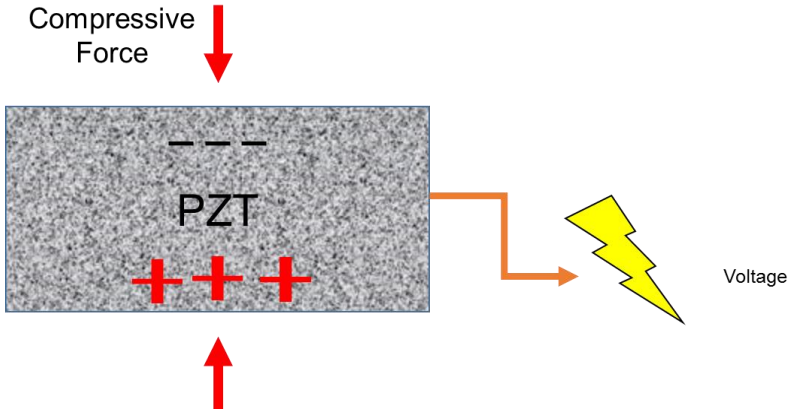

Figure 5: Schematic of basic mechanism of PZT materials.

phenomenon, PZT materials are often used as electrical generators in many applications.[27],[31]–[34] One such application is in development of orthopedic medical implants that undergo dynamic loading.[31] With consideration of the spine specifically, it undergoes dynamic loading, while axial compressive forces act upon the intervertebral bodies.[35]

With considerations of dynamic loading and compressive forces on spinal interbodies and its potential to replace an external battery pack, PZT has been explored as a material choice for spinal implants. For example, a layered piezoelectric material containing fibers embedded in epoxy was developed and when electromechanically tested, generated power, thus having potential use for spinal fusion stimulation.[34]

1.3.1 Piezoelectric Properties + Power Generation

Although PZT has been shown as a potential generator for medical implants, its efficiency, storage, and power output has not been refined.[31] Because of the lack of refinement, studies have been performed to determine such properties of the PZT material. One study used a PZT element embedded inside of spinal fusion implant which was subjected to low sinusoidal frequencies (1-10 Hz) with load amplitudes of 400 to 3000 N, while displacement and voltage data were also acquired from the implant during the cycles.[31] It has been found in both theoretical and experimental studies that the conversion of mechanical power into the raw electrical energy was possible and using PZT inside of an implant undergoing cyclic loading, produced enough power to run small clinical electronics.[31], [33]

1.3.2 Stacked Generator, Power Generation, & Compliant Layers

Designing the structure of a PZT generator is highly dependent on its direction of loading during usage. The two main types of PZT generators have already been studied by Platt et al. to investigate the differences between a monolithic generator (single layer) and a stacked generator (multiple layers).[32] Based on knowledge from Platt et al., power generation was investigated using the idea of a stacked generator in the form of a stacked, macro fiber PZT composite spinal interbody device.[34] By developing a composite material, the toughness of the PZT material was increased with a tough polymeric matrix.

It was predicted that adding compliant layers would ultimately toughen, yet maintain the desired power generation necessary for the spinal fusion application. The compliant layers were made of epoxy, using thicknesses of 0.0 mm, 0.4 mm, and 0.8 mm. The hypothesis was that the addition of a compliant layer in between the layers of the stacked PZT discs (traditional stacked generator) would increase the power generation due to the ability of the compliant layers to allow the brittle PZT to deform more readily when stacked in between each disc due to their anisotropic strength as a laminate layer. This has previously been highly theorized and tested with laminates of different phases (laminate composites).[36] Therefore, the strength of the epoxy should enhance the other discrete phase (PZT) because it allows for the force to be distributed throughout the laminate composite in more directions as compared to a traditional stacked generator.[36] In a traditional stacked generator, without any matrix or compliant material, the PZT discs isotropically respond to a compressive load. Thus, adding a

compliant layer allows anisotropic behavior that can be added to the isotropic stacked generator.

The addition of the compliant layers should result in improved fracture toughness as compared to the traditional stacked generators. Energy absorption of the force exerted on the material during loading can be absorbed by the anisotropic compliant layers.[37] This contrasts with the PZT discs alone, as they are a brittle material and do not absorb fracture energy as efficiently as the compliant layer. Therefore, the overall generator should exhibit improved fracture properties with the addition of a compliant layer compared to the traditional stacked generator.

1.4 Mechanical Testing

Mechanical testing of materials is vital to the success of an implant because its function is directly related to its material properties. It is necessary to determine whether the PZT composite with compliant layers is tough enough and how much load it can withstand before permanently deforming. Two common tests to examine both properties are tensile testing and fracture toughness testing; both of which have been widely used in testing many other materials but not the specific combination of materials being investigated.

1.4.1 General Tensile Testing

Tensile properties of plastics can be determined using ASTM D638-10, which specifically covers plastic materials that can be reinforced, or non-reinforced (Figure 6).[38] The application of this standard is relevant when considering the PZT composite containing discs stacked or discs stacked with intermediate epoxy layers. This is especially important because PZT material by nature is weakest in tension than in

compression. Therefore, the tensile test can test for the materials worst-case scenario of failure for the PZT material. Tensile testing reveals a specific property of the material known as the Young's Modulus. With a tensile test, stress (force applied over an area) versus strain (change in length over original length) can be obtained. Stress and strain plotted can be used to calculate information about the materials' ultimate tensile strength, the point at which the material will fail under a certain load, or yield strength, the load at which the material will begin to undergo plastic deformation. The stress and strain curve also reveals a region of elasticity, where the plastic material deforms under

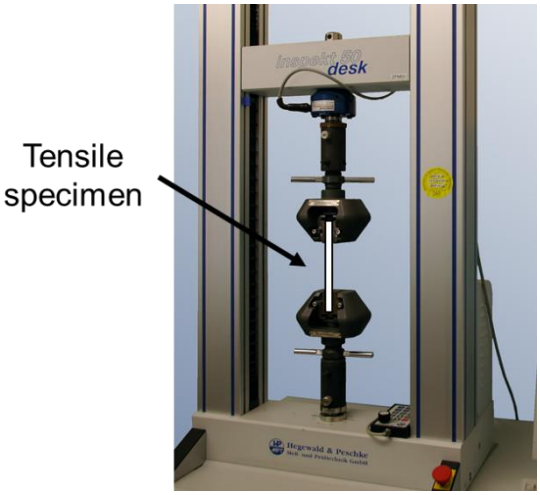

Figure 6: Schematic of tensile testing set-up. (Public Domain, modified for use)

the applied stress and can still return to its original state. The region of elasticity is where you determine the Young's Modulus, which is the slope of the linear region. Knowing the Young's Modulus of a composite material is important because it can prevent loss of the materials' primary function.[39]

Like the original fiber composite material developed by Goetzinger et al., Dent et al. performed a study examining the volume fraction of PZT fibers compared to the

volume fraction of the matrix using an ISO standard equivalent to ASTM D638-10 that was modified.[27],[39] The modification in Dent et al. consisted of attaching aluminum end tabs to the ends of the specimen to allow for better grip and to maintain the integrity of the section of material that is to be tested.[39] Without adherence of end tabs with a different material than the composite itself, there would be composite damage risks associated with following an unmodified ASTM D638-10 or equivalent ISO standard. Thus, with Dent et al.'s modification, the composite material was successfully tested in

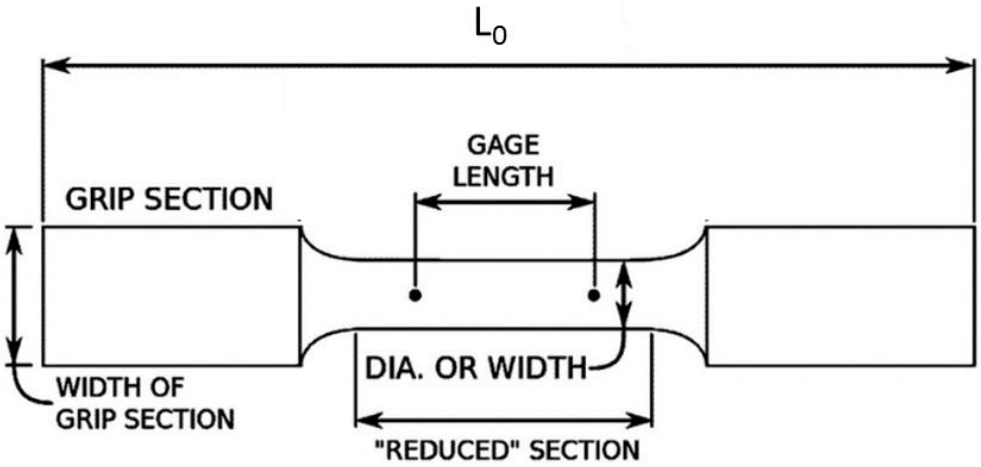

Figure 7: Image of a traditional tensile testing specimen for plastic materials, note that typically this specimen geometry for tensile testing would be made entirely of one material, L_0, gage length, diameter, and width are based on ASTM D638-10. (Public Domain, modified for use)

tension without damaging the composite material of interest. Modification also eliminates the need to create large specimen purely made of composite material (Figure 7). This experimentation, along with others, demonstrates that modifications to specimen fabrication allows for a more valid tensile test.[39], [40] A valid and applicable test is vital in insuring that the failure mechanisms of the material is understood prior to being used, especially in a medical implant application.

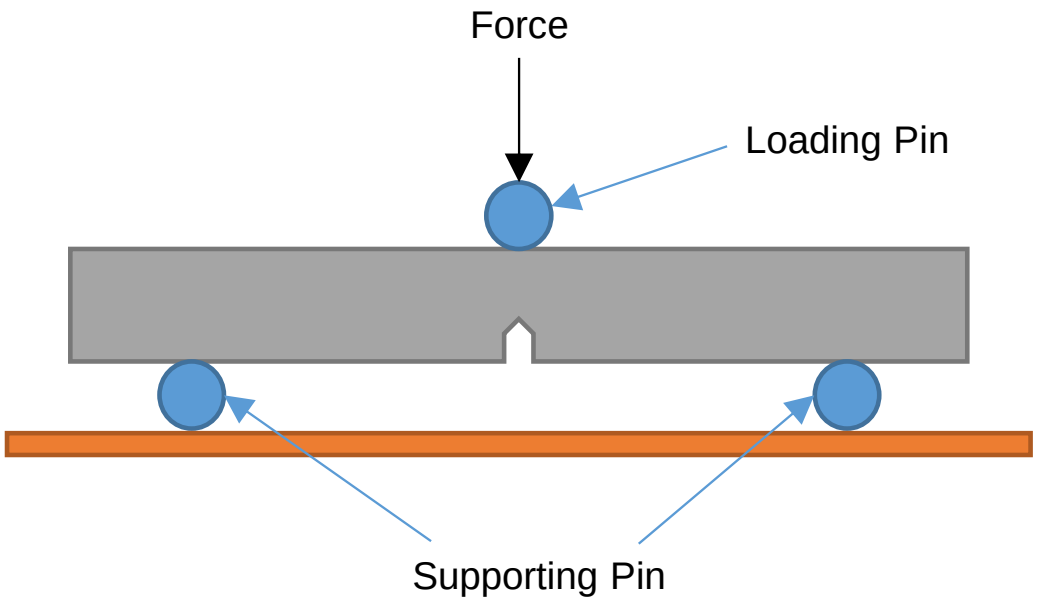

Figure 8: Schematic of a single-edge-notch bend specimen undergoing a fracture toughness test.

1.4.2 General Fracture Toughness

As described by ASTM D5045-99, a plane-strain fracture toughness test can characterize the fracture toughness of plastics in terms of its critical-stress intensity factor, K_{IC}, using a single-edge-notch bend (Figure 8).[41] The critical-stress intensity factor is what represents the fracture toughness of a material and measures the stress necessary to propagate a sharp crack created. A higher fracture toughness value describes a material that will exhibit ductile fracture when a crack is present in the material, and is indicative of a higher resistance to fracture (resistance to crack propagation). A low fracture toughness value describes a material that will exhibit brittle fracture when a crack is present in the material, and is indicative of a lower resistance to fracture.

The resistance to cracking is related to the material's ability to deform plastically, while absorbing energy away from the crack tip prior to failing.[42] This happens at the front of the crack tip where there is an area known as the crack tip energy field that is dictated by the radius, "r" (Figure 9). In consideration of a medical implant application, it is desirable for the material to exhibit a higher fracture toughness value, in which it is highly resistant to cracks propagating through the material.[43]

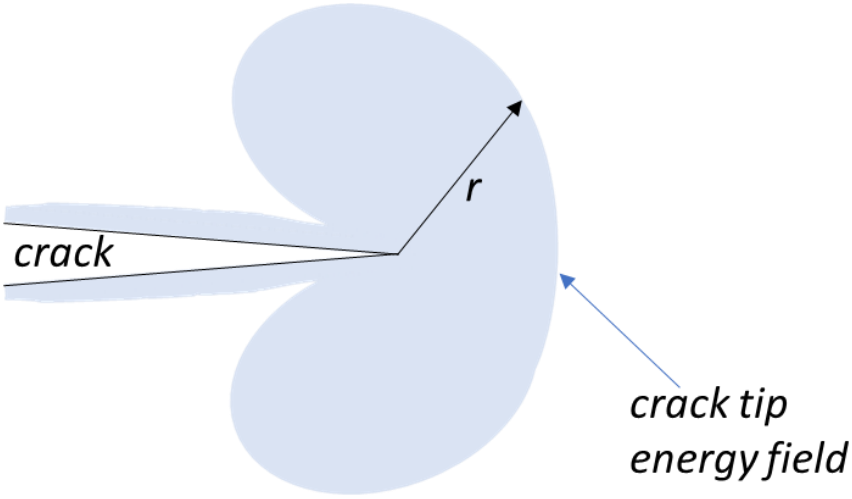

Figure 9**:** Schematic of a crack within a plastic material and the crack tip energy field in front of the tip of the crack, where the radius determines the area in which the material can absorb energy to prevent crack propagation.

A fracture toughness test helps show whether the composite material developed, with compliant layers, can resist failure due to cracking compared to just PZT discs (by nature is brittle because it is a ceramic). Too often strength is the focus of the study and fracture toughness is ignored. The material's fracture toughness depends on the ability of a material's microstructure to enable toughening mechanisms (mechanism of crack deflection) prior to the crack or after the crack tip.[42],[44] Therefore, utilization of fracture-mechanics to characterize materials is vital to the success of the materials chosen for implant development.

1.5 General Composite Theory

A composite material is composed of a fiber that is high in strength and stiffness, but is brittle, and combined with a matrix material that is usually weaker, but tough and requires reinforcement by the fiber.[45] The benefit of the composite material is that the brittle nature of the fibers should be supported from buckling due to stress concentrations, when there is a matrix material that surrounds the fibers. The combination of both materials should increase the toughness compared to just the brittle fibers themselves, as can be seen in Figure 10. The composite material can be modified to resist forces in a specific direction. Fiber alignment within the matrix can highly dictate the material's toughness. Using this concept, a composite material is highly appropriate for use in a spinal fusion application. Similar principles have been used in other applications using carbon nanotubes aligned with the direction of the force applied, thereby allowing the fibers to distribute the shear stress to the matrix.[46], [47]

However, designing a composite material in which the fiber is a singular disc (large cross section of a fiber), embedded into a polymeric matrix can prevent it from failing compressively due to stress concentrations. If the stacked generator was not a

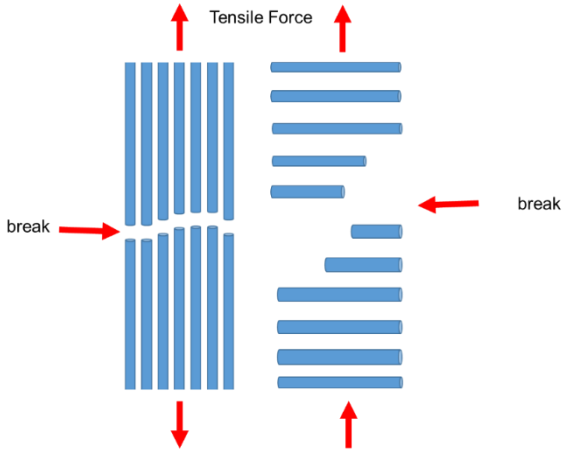

Figure 10: Schematic of failure of fibers without a matrix to support, when tensile stress is applied.

composite, compressive failure would be more likely due to the larger stress concentrations around the PZT within a polymeric matrix (Figure 11). With compliant layers, the large stress concentration is distributed throughout all the layers present within the generator (Figure 11). Therefore, a composite material with PZT discs could be used to develop a spinal fusion implant.

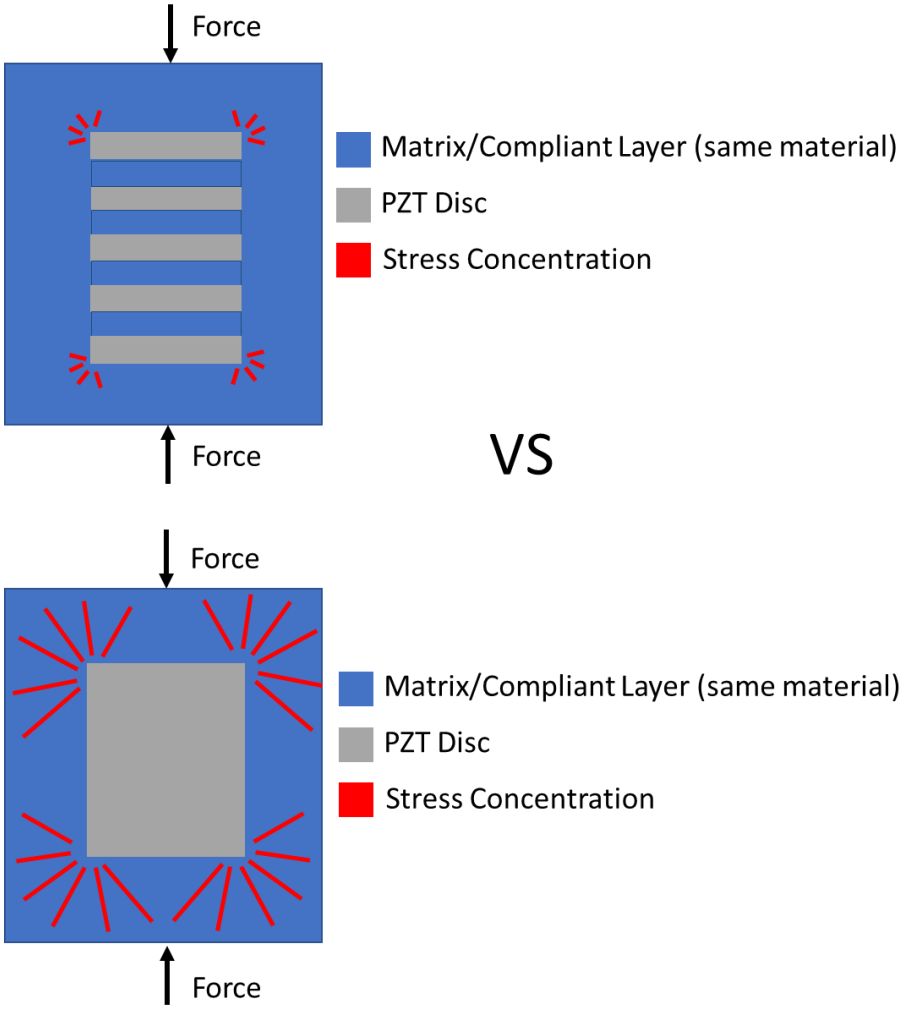

Figure 11: Schematic comparing a full PZT stack versus compliant layer PZT stack undergoing compressive forces. The schematic shows how the stress concentrations are more distributed across the compliant layer PZT stack than the one without compliant layers.

1.6 Summary

It is crucial to develop a spinal fusion implant, in which the material can withstand the loading of the body. By examining the material properties of a newly developed stacked PZT generator with compliant layers, the overall toughness and resistance to deformation can be understood. To determine an appropriate material for a spinal fusion implant, the mechanical properties of the newly designed composite material must be characterized and compared to a tough control material (epoxy).

Chapter 2: Study

2.1 Introduction

To conduct fracture toughness and tensile testing on the composite inserts, it was necessary to modify the ASTM standards used to fit the limitations of the specimen size. Instead of using a full-length coupon for both the fracture toughness test and the tensile test, epoxy resin was attached to the specimen to meet geometry and size requirements as designated by the ASTM standards. Overall, the following study investigated the effect of the compliant layer on the composites strength and toughness, as well as in comparison to epoxy. The average fracture toughness and Young's modulus were measured for these two different materials.

2.2 Methods

2.2.1 Development of Test Specimen

Two piezoelectric composite inserts with varying compliant layer thickness were used for comparison. The first insert (named the "0.4 mm specimen") consisted of a PZT composite containing five layers of 0.4 mm PZT (10 mm x 0.4 mm, STEMiNC, through the thickness poled) and four layers of 0.4 mm cured epoxy slices (EPO-TEK®301), stacked in alternation. The second insert (named the '0.0 mm specimen) to be tested consisted of five layers of 0.4 mm PZT (10 mm x 0.4 mm, STEMiNC, through the thickness poled) stacked upon each other. The 0.0 mm specimen did not contain compliant layers, while the 0.4 mm specimen did contain compliant layers. These inserts were electrically connected using thin coppers strips and medical grade

conductive epoxy (EPO-TEK® H20E) to insure the layers were electrically parallel and mechanically in series (Krech, *et al*).

It is important to note that the composite inserts were tested electromechanically, using a MTS MiniBionix 858 with self-aligning platens, to insure the inserts were electrically active. In addition, the inserts underwent ultrasound testing for a parallel study. Both tests determined successful fabrication of an insert by measuring if the insert gave power. After the electromechanical tests were performed, inserts were cut into smaller sizes to make two types of specimen geometry. Each insert was cut into five half specimens used for tensile testing (n = 5) and five half specimens for fracture toughness (n= 5). The following steps detail the modification of the ASTM 5045-99 for in-plane strain fracture toughness and ASTM D638-10 for Tensile Properties of Plastics.[38), (41)]

2.2.2 Tensile Specimen Fabrication

As mentioned previously, each insert specimen was cut in half using a thin band saw through the thickness, so that two halves were produced per insert (Figure 12).

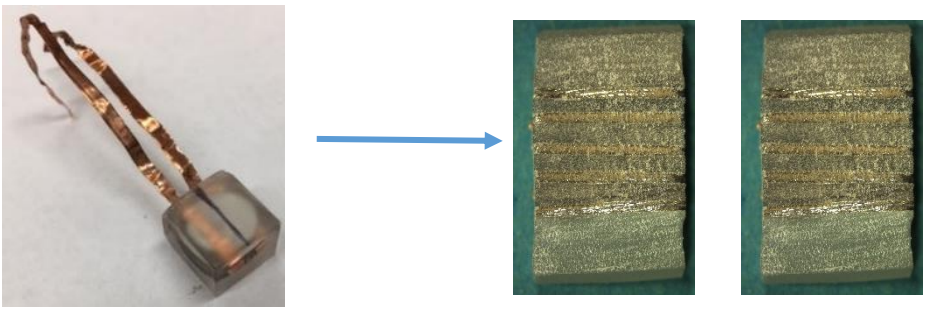

Figure 12: Image of a single insert cut into two halves, one half used to create the tensile specimen, and the other used for fracture toughness.

Each specimen was then measured to insure a width, *W*, (critical dimension) of 6 mm and a thickness, *T*, (critical dimension) of 3 mm (Figure 13) (Table 1).

Table 1: This is a table listing dimension limitations from ASTM D638-10 for Tensile Properties of Plastics. The specific specimen type used and then modified was Type II, dimensions can be referenced back to dimension table in ASTM D638-10.[38]

Dimensions	Value (mm)
W-width of narrow section	6
L-length of narrow section	57
WO – width overall	19
LO- length overall	183
G – Gage length	50
D – Distance between grips	135
R - Radius	76

If measurements were slightly larger due to excess epoxy, the specimen was carefully and gently sanded down using a Dremel® so that the width and thickness was precise. It was also insured that during sanding, the surface was as flat as possible to allow for proper edge alignment with the mold. A laser cut Poly(methyl methacrylate) cast, with dimensions meeting requirements of Type II specimen in ASTM D638-10, was used as

Figure 13**:** Image of mold with half specimen placed and properly centered into Dragonskin 10 (Smooth- On, Inc., Easton, PA).

the cast with Dragonskin 10 (Smooth- On, Inc., Easton, PA) to create the tensile testing specimen mold.[38] With this mold, one of the halves of the insert was placed into the

mold so that it was centered along the narrowed neck region (gage length) of the dog bone shaped cavity (Figure 14).

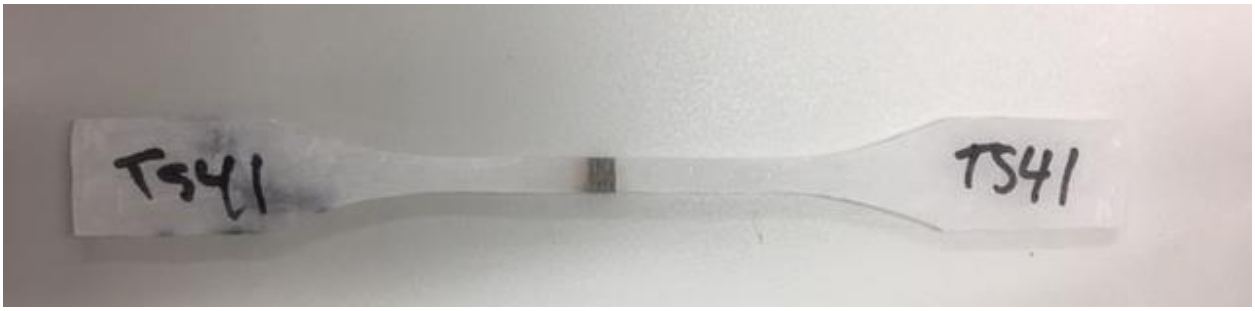

Figure 14**:** Example of a full tensile specimen with a 0.0 mm insert after removal from tensile specimen mold.

The half was placed in the mold cavity so that the layers would be transverse to the applied force during testing **(**Figure 15). Epoxy was made using EPO-TEK®301 Part A and Part B with a mix ratio of 20:5 to achieve a total weight of approximately 8 grams. This was then used to fill the space around the half specimen in the pocket so that the uncured epoxy was level with the surface of the half now placed in the mold. This idea of using a surrounding material to the material of interest was inspired by a study examining the effect of piezoelectric fiber volume effects using metal dog bone tabs attached to the material of interest for tensile testing.[39]

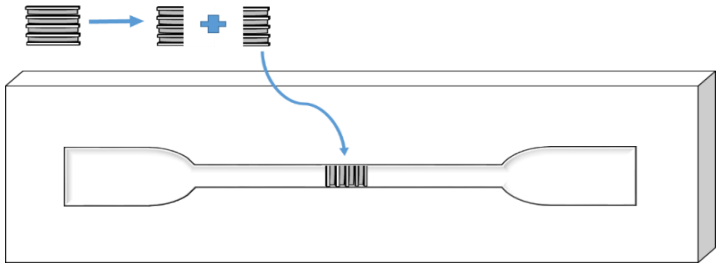

Figure 15**:** Schematic of correct placement of half specimen in tensile testing mold.

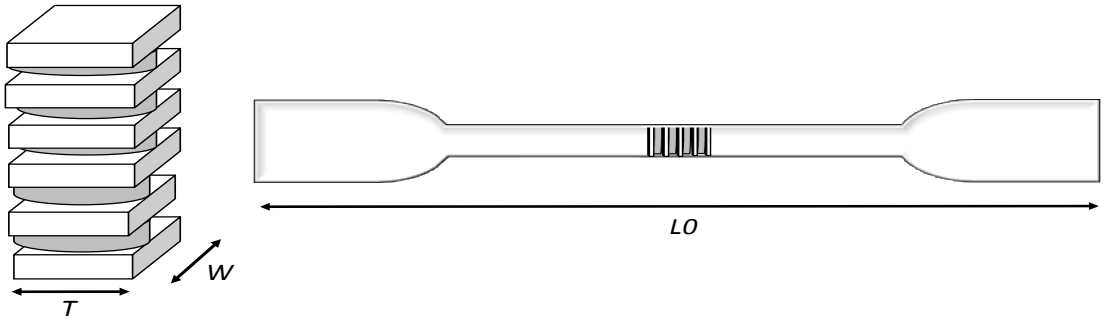

Figure 16**:** Exaggerated schematic of critical insert specimen dimensions after insert is cut in half for tensile testing, where *T* is thickness, *W* is the width of the gage length region, and *L0* is the overall length.

The entire mold with the embedded specimen was then allowed to cure for 24 hours at room temperature, and then oven cured at 65° C for two hours before removing from the oven. After removal, dimensions were measured again to ensure that the dimensions were still accurate, if not (due to flash of the material/too much material poured into the mold) a Dremel® was used to help achieve the correct dimensions as aforementioned. An example of the final specimen can be seen in Figure 16. Final average specimen dimensions and standard deviation can be seen in Table 2**.**

Table 2: This table contains the average dimensions and standard deviations for the different types of tensile testing specimen used during testing. The narrow region is the average width of the gage length of the specimen. The averages were from a sample size of n = 5 for each sample type.

Sample Type	**Average *W*** (width of narrow region, mm)	**STD** (mm)	**Average *T*** (thickness, mm)	**STD** (mm)
Control	6.02	0.01	3.03	0.03
0.0 mm	6.00	0.01	3.02	0.01
0.4 mm	6.01	0.02	3.01	0.01

This entire method was repeated for all 0.0 mm inserts, 0.4 mm inserts, and. Control specimen were made in a similar manner without needing to embed them as the control samples were all made of pure epoxy. This full method was implemented until a sample size of n = 5 for each type of insert was achieved.

2.2.3 Fracture Toughness Specimen Fabrication

For fracture toughness specimen, using ASTM D5045-99, the SENB (single edge-notched beam) was used as the primary configuration of the specimen.[41] This geometry was chosen due to its ease of manufacturing compared to the CT (compact tension) configuration. Additionally, SENB allowed for the insert to be cut into two halves, allowing one to be used in tensile testing and the other remaining half for fracture toughness.

Again, each insert was cut in half, one half used specifically for fracture toughness. The width (*W*) of the to-be embedded insert was insured to be 10.00 mm and the thickness (*B*) insured to be 5.00 mm. Again, precision of dimensions and a level specimen surface was ensured by using a Dremel® to sand the specimen carefully and gently if necessary. Laser cut Poly(methyl methacrylate) material, cut with the correct necessary fracture toughness dimensions based on ASTM D5045-99, was used as the cast with Dragonskin 10 (Smooth- On, Inc., Easton, PA) to create the fracture toughness testing specimen mold.[41] It is important to note that during creation of the dimensions using ASTM D5045 -99 critical dimensional restraints had to be followed. Specifically, the specimen width (*W*), with the insert embedded as well, must meet the criteria of being two times the thickness (*B*) of the specimen (Figure 17).

Figure 17: Image of full fracture toughness specimen (un-sanded, 0.4 mm) after removal from mold.

With the mold created using the laser cut material, one of the halves of the insert was placed into the mold so that it was centered and aligned with the top edge within the rectangular pocket of the mold (Figure 18).

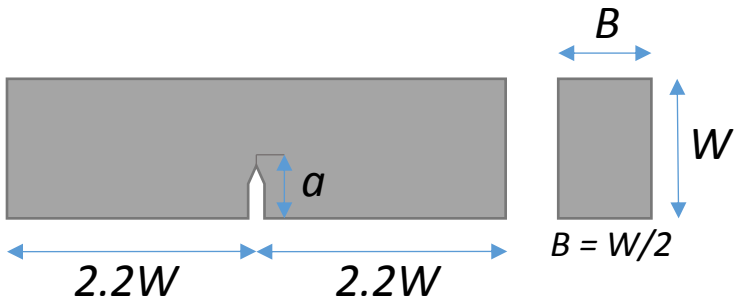

Figure 18**:** Schematic of dimensional criteria for the SENB configuration used in developing the fracture toughness specimen.

The half insert was placed so that the alignment of the discs allowed for the development of a crack to be along the interface of the composite. Epoxy was made using EPO-TEK®301 Part A and Part B with a mix ratio of 20:5 to achieve a total minimum weight of approximately four grams, which is enough to be used for up to two specimens. It was used again to fill the surrounding area of half insert in the fracture

toughness mold, enough so that the uncured epoxy was level with the top surface of the half insert. The entire fracture toughness mold was then allowed to cure for 24 hours at room temperature, and then oven cured for two hours at 65° C for two hours before removing from the oven. An example of the final specimen can be seen in Figure 19.

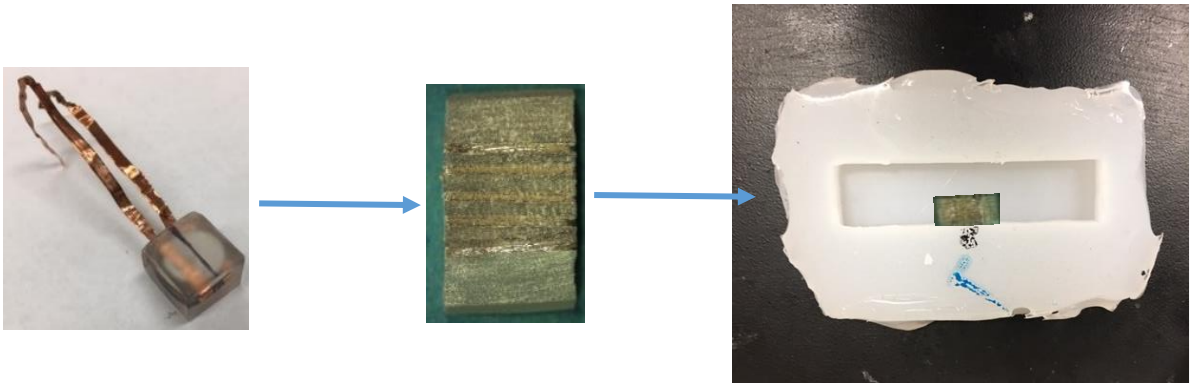

Figure 19**:** Image of mold with half fracture toughness specimen placed and properly centered into Dragonskin 10 Smooth- On, Inc., Easton, PA) mold for fracture toughness testing.

Final steps to developing the fracture toughness specimen included starting the initial crack (*a*); average values can be found in Table 3. ASTM D5045- 99 requires that the results of the specimen tested are only valid if it meets the critical size criteria, as well as a crack length ("a") between a maximum length of 5.5 mm and a minimum of 4.5 mm:

$$0.45 < \frac{a}{w} < 0.55$$

Notice that the limitations are dependent on the width of the material. Because the width was to be 10 mm, "a" could not exceed the upper and lower bounds multiplied by 10.

First, the band saw was used to notch the specimen, on the half that was cured epoxy, so that a thin razor blade could then be used to saw the crack to meet length requirements. Rather than using a tapping motion of the razor blade, a gentle sawing

motion was used because there was much more control in insuring the crack did not exceed the maximum crack length requirements. The crack length could not be controlled to a specific length, but was developed to stay within the specified range as designated by ASTM D5045-99.[41]

The crack was sawed to length towards half of the specimen with the embedded PZT insert (Figure 21). An example of the final initiated crack can be seen in Figure 20**.**

These steps were repeated with all the 0.0 mm and 0.4 mm fracture toughness

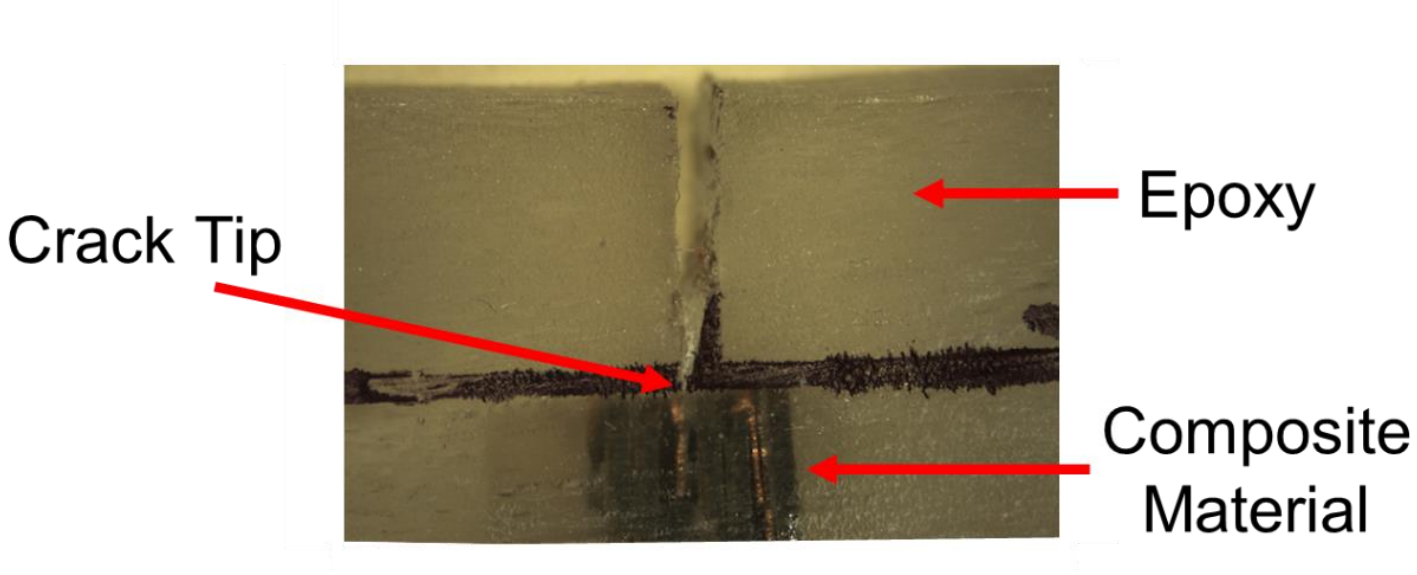

Figure 20**:** Close-up image of crack initiated into final fracture toughness specimen (0.0 mm).

specimen. The controls followed the same methodology, with the exception that there was no embedding necessary due to the control being made fully of epoxy. The overall methods were followed until a sample size of n = 5 were developed for each specimen type. Average fracture toughness specimen dimensions, as well as, crack length and standard deviations can be seen in Table 3.

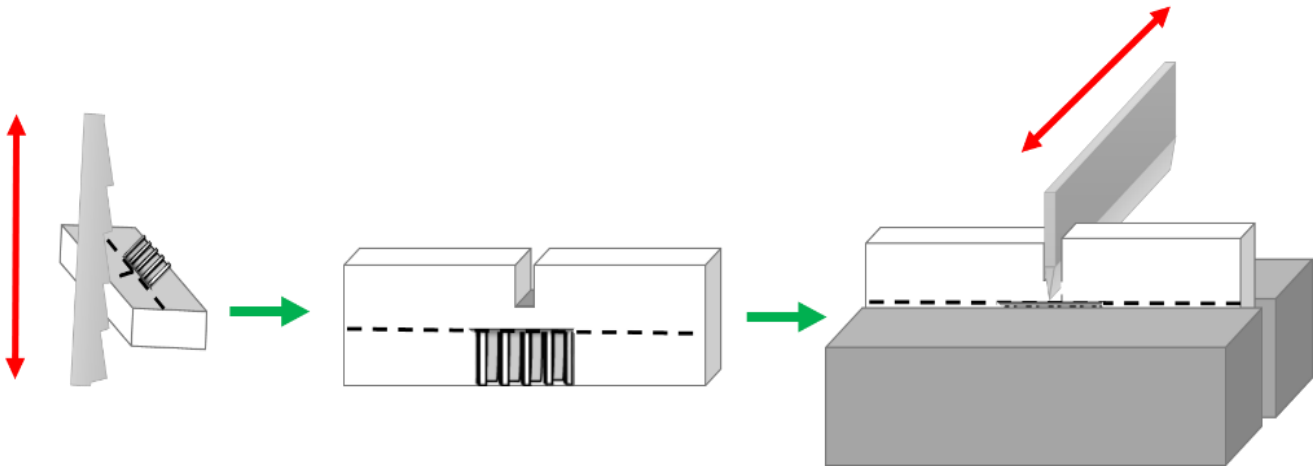

Figure 21**:** Schematic of crack initiation into fracture toughness specimen 1) band saw to notch specimen 2) notch created to end prior to PZT material 3) razor blade using sawing motion to initiate final crack.

Table 3: This table contains the average dimensions and standard deviations for the different types of fracture toughness specimen tested, the values are reported to two decimal places as specified by the ASTM D5045-99. Each average is from the sample size of n=5 for each sample type.

Sample Type	**Average *W*** (height, mm)	**STD** (mm)	**Average *B*** (thickness, mm)	**STD** (mm)	**Average *a*** (initial crack length, mm)	**STD** (mm)
Control	10.01	0.03	5.01	0.01	5.02	0.03
0.0 mm	10.02	0.02	5.01	0.01	5.16	0.15
0.4 mm	10.01	0.01	5.00	0.01	5.36	0.15

2.2.4 Experimental Measurements and Data Collection

Testing was performed using an MTS Criterion® Series 40 Model 45 for both tensile testing and fracture toughness of the three types of specimen. For tensile testing, Advantage Wedge Grips were used and a Laser Extensometer (Electronic Instrument Research, Irwin, PA) connected to the MTS to measure the specimen's

change in length. Each tensile specimen was prepared with silver reflective tape placed along the top and bottom edge of the specimen, where there is a clear transition between the insert to the epoxy (Figure 22). To ensure that results reflected strain on just the composite material and not including the surrounding epoxy, reflective tape was not placed to mark the entire narrow region (gage length) of the tensile specimen, since the material of interest was much smaller than the entirety of the gage length. Therefore, reflective tape was only applied around the material of interest along the tensile specimen (Figure 22).

Figure 22**:** Example image of final tensile specimen conveying placement of silver reflective tape.

Test set-up parameters include a displacement of 5 mm/min and data acquisition rate of 100 Hz. Each tensile testing specimen was clamped into the wedge grips and stretched until failure in uniaxial tension, while the laser recorded change in length (Figure 23). Stress and strain data was collected from the tensile test. Then a linear regression fit in Microsoft Excel was used to fit the elastic region of the data to determine elastic moduli of the specimen by using the linear regression slope. This was

repeated for each set of 5 specimen type. Average elastic moduli and standard deviation were calculated for each specimen type.

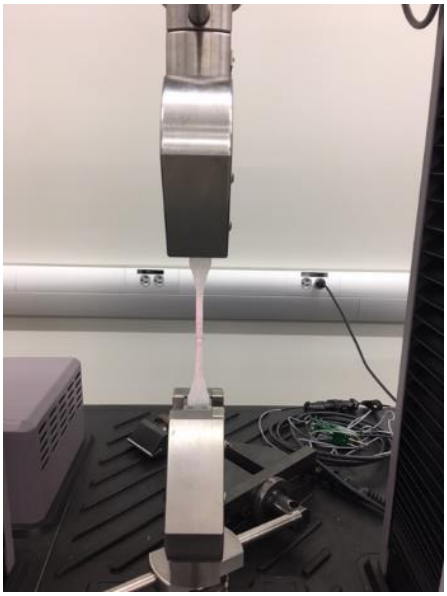

Figure 23**:** Image of final tensile specimen with silver reflective tape stretched inside of wedge action grips using the MTS.

For fracture toughness testing, a three-point bending rig was used to obtain data for fracture toughness (Figure 24). Each specimen was loaded into the rig according to ASTM D5045-09. Testing parameters for fracture toughness included a loading rate of 10 mm/min, as suggested by ASTM D5045-09, and a data acquisition rate of 100 Hz. Bending was performed until a break was detected in the specimen. Load and displacement data was collected from the single-edge-notch bend test. The data was then used to calculate K_{IC} (plane-strain fracture toughness) following the guidelines of ASTM D5045-99 with Microsoft Excel**.**[41] An average fracture toughness value and standard deviation was calculated for each specimen type.

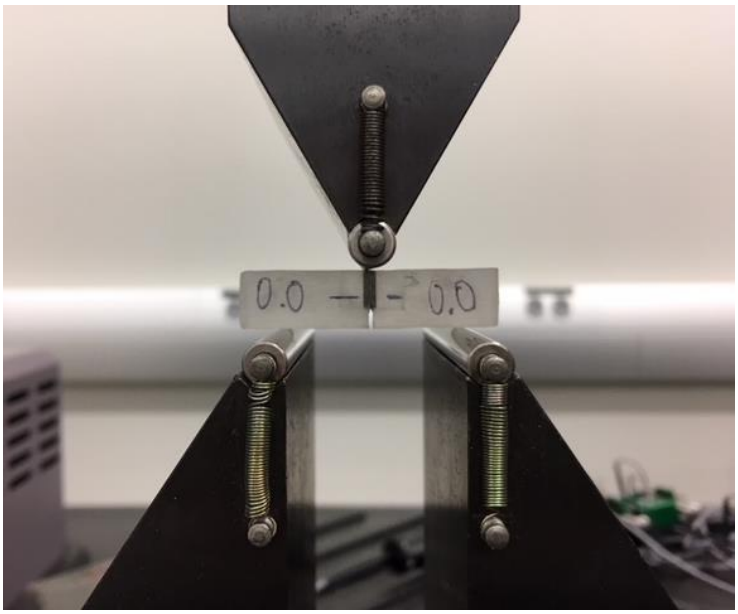

Figure 24: Image of fracture toughness specimen (0.0 mm) set-up in MTS bending grips.

2.2.4 Statistical Analysis

Statistical analysis for the results was performed using SAS (Statistical Analysis Software) (Appendix A). For all three fracture toughness specimen type, statistical significance of specimen type on the average fracture toughness was compared among the material types, as well as, to the control type specifically using an ANOVA with a significance level of $\alpha = 0.05$. In addition, a Tukey-Kramer post-hoc test was used to account for multiple-comparisons and their pairwise significance. The alternative hypothesis utilized the sample mean as well.

2.3 Results

2.3.1 Tensile Testing Analysis

The effects of the compliant layers on the composite material, no compliant layers, and the control with plain epoxy was measured under uniaxial tensile load. The following results display the tensile tests performed on the specimen types. Figure 25 displays a sample stress vs strain curve from the control tensile testing specimen type, specifically Control specimen 4.

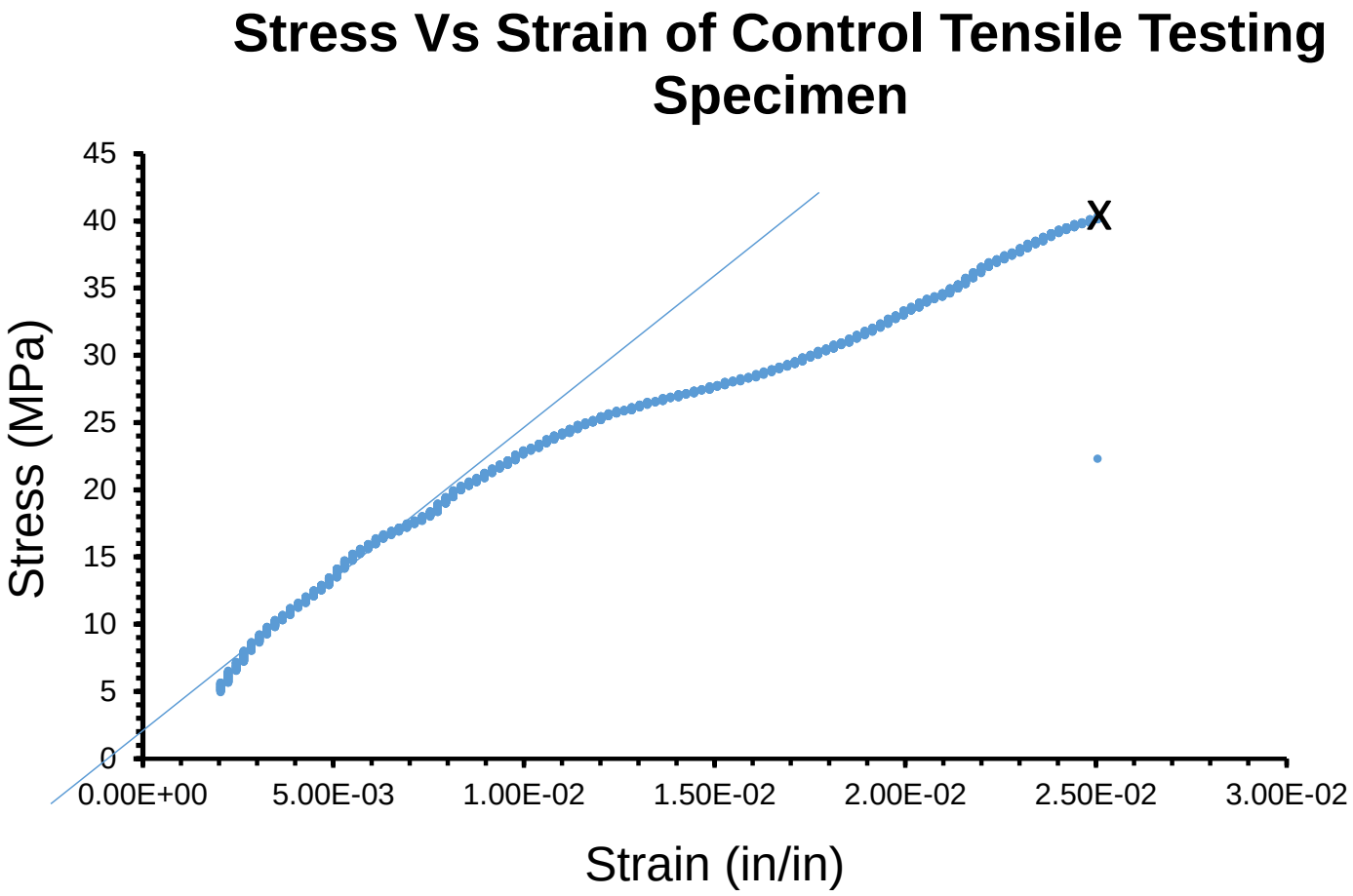

Figure 25**:** Graph of example stress vs strain for control (epoxy) tensile testing specimen with linear fit applied.

Figure 26 displays the elastic region of one of the control sample's stress versus strain curve. Within the figure, the linear fit applied to the elastic region to determine the Young's Modulus is displayed. The example slope of the linear elastic curve is the Young's Modulus for the respective specimen mentioned previously. Additionally, Table 1 displays the Young's Modulus (MPa), obtained from linear fit of stress and strain, for each control sample, as well as, the overall sample average and standard deviation.

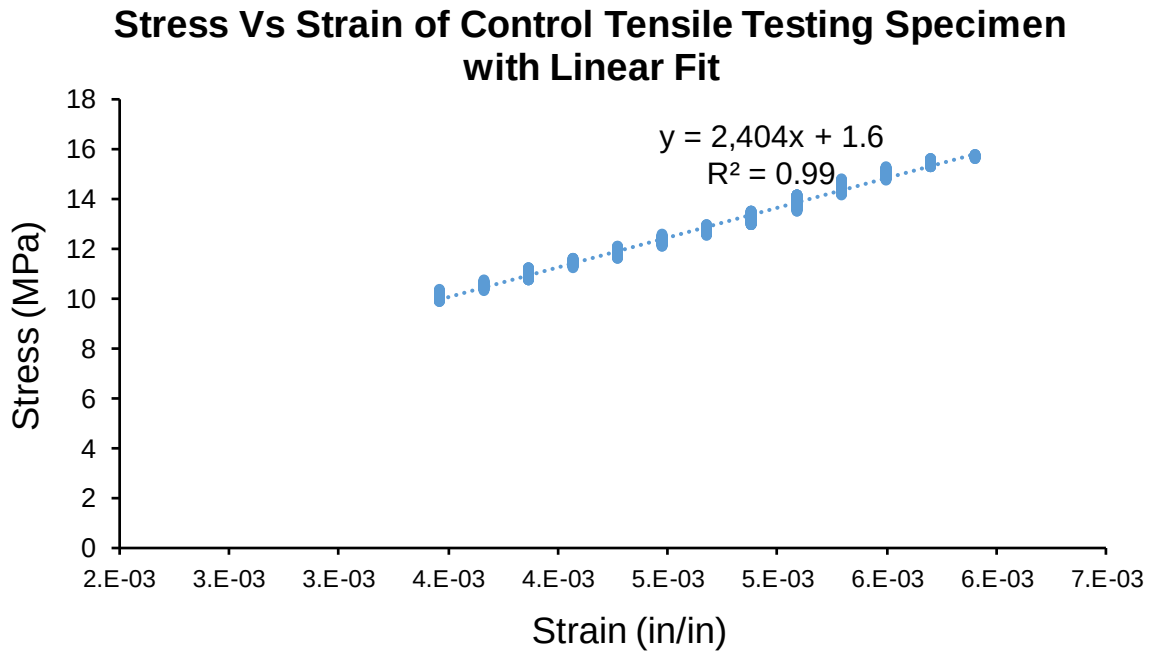

Figure 26: Graph of example elastic region stress vs strain for control (epoxy) tensile testing specimen with linear fit applied and R^2 value.

Table 4: Young's modulus values obtained from linear fit of stress vs strain curves, sample average and standard deviation are also displayed.

Sample	Young's Modulus (MPa)
Control 1	2782
Control 2	1908
Control 3	1993
Control 4	2404
Control 5	2167
Average	2251
Standard Deviation	± 315

2.3.2 Fracture Toughness Analysis

The effects of the compliant layers, no compliant layers, was measured compared to the control specimen with only epoxy using three-point bending to ultimately determine fracture toughness. The following results display the sample average fracture toughness values and standard deviations for each specimen type (Figure 27). Average values were calculated from load versus displacement data acquired during fracture toughness testing, as mentioned previously.

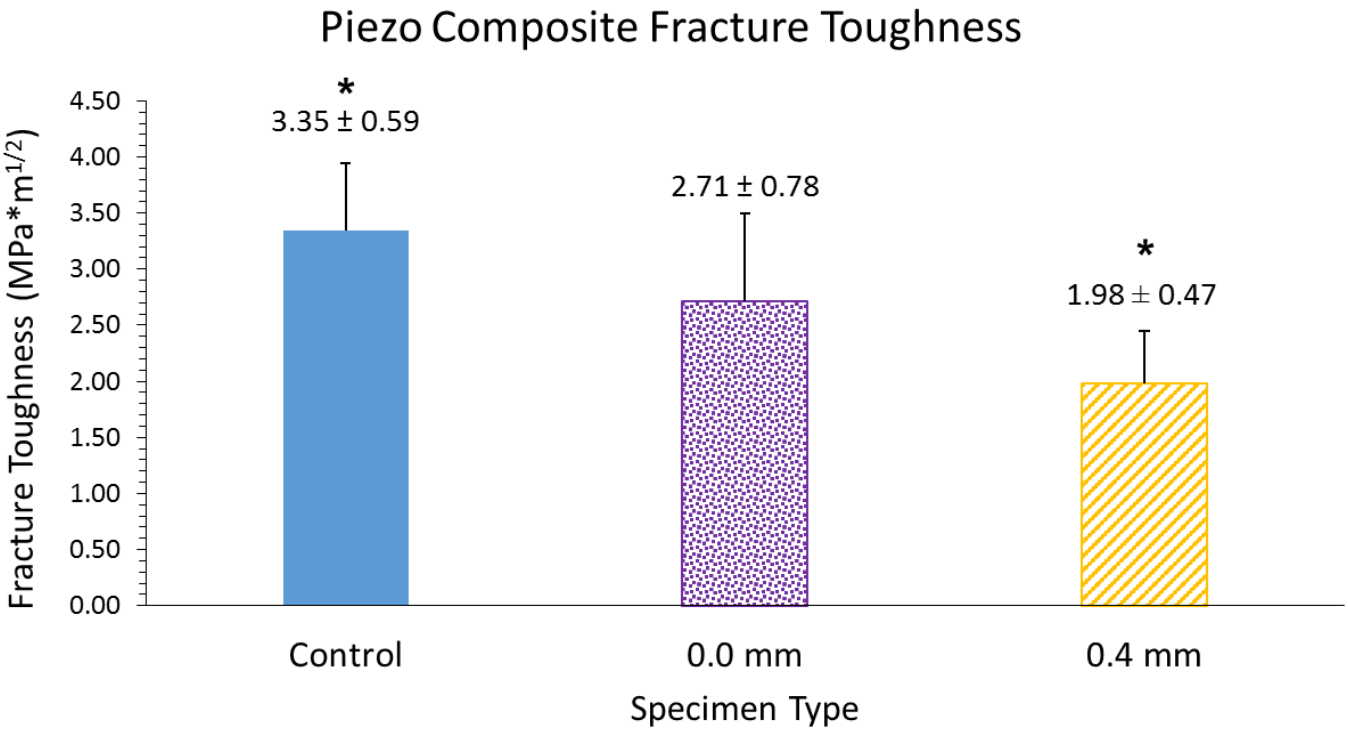

Figure 27: Comparison of sample average fracture toughness values for each specimen type, including positive standard deviation. **Significant difference between each other.*

Based on Figure 27, the control sample exhibited the highest average fracture toughness of 3.35(0.59) MPa·$m^{1/2}$, while the second highest fracture toughness was exhibited by the 0.0 mm specimen with an average fracture toughness of 2.82(0.78)

MPa·$m^{1/2}$, and the lowest average fracture toughness was exhibited by the 0.4 mm specimen with a fracture toughness of 1.98(0.47) MPa·$m^{1/2}$.

The one-way ANOVA yielded presence of significance, $P < 0.05$, between material type and the material's fracture toughness. Tukey-Kramer pair-wise post hoc testing revealed that there is no significant difference in fracture toughness (1) the control specimen and (2) the 0.0 mm specimen and (3) the 0.4 mm specimen. However, the 0.4 mm specimen is significantly different from the control specimen**.**

2.4 Discussion

The purpose of this experimental study was to determine the material properties of the material used in the spinal fusion insert. The fracture toughness and elastic modulus of the 0.0 mm composite material and the 0.4 mm composite material were compared to medical grade epoxy to reveal the effects of adding a compliant layer.

2.4.1 Tensile Testing Analysis & Specimen Failure

Examining the results of the tensile testing elucidates that there is an inability to calculate the Young's Modulus from the data acquired for both the 0.0 mm and the 0.4 mm composite specimen (Figure 28).

A proper stress-strain curve, containing an elastic and plastic region and an evident failure point, could not be produced by the load and displacement data acquired. Because the stress-strain curve could not be produced, a linear fit could not be used to fit elastic region to determine a modulus of elasticity with its slope. This was true for all data for both specimen types, except for the control specimen.

Although Young's Modulus could not be determined for the 0.0 mm and 0.4 mm tensile testing specimen, it could be determined for the control epoxy tensile testing

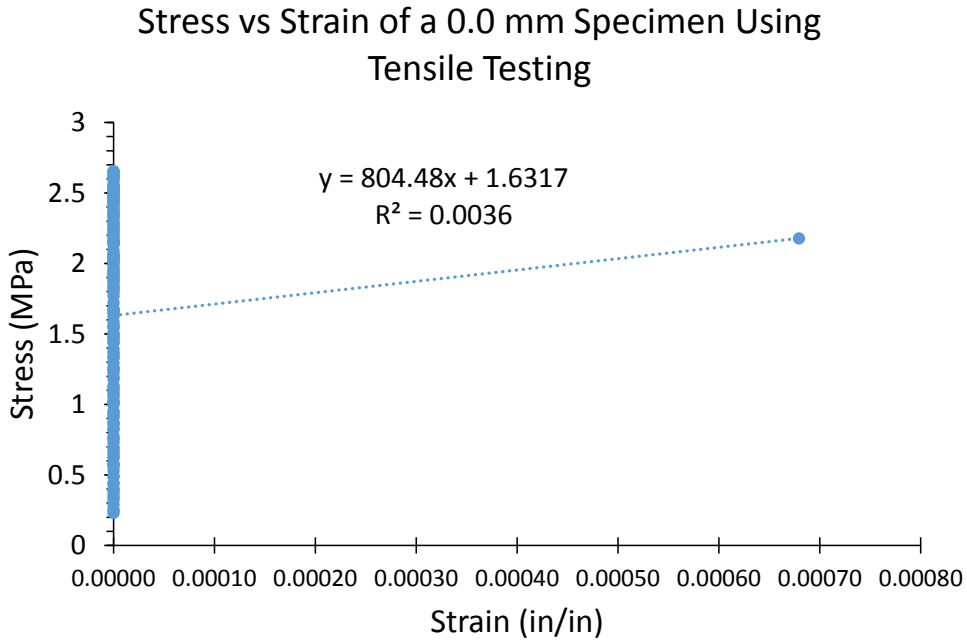

Figure 28: Sample graph of stress versus strain of a 0.0 mm tensile testing specimen, revealing the lack of change in strain. The clustered values represent repeated strain values even though stress is increasing.

specimen. Stress-strain curves with a linear fit, as seen in the section 2.3 Results, display a value of E = 2251 MPa with a standard deviation of 352 MPa. Comparing this value to the reported Young's modulus of epoxy by EPOTEK (E = 2258 MPa), there is a 0.31% difference between the values.[48] The experimental Young's modulus of just epoxy was precisely measured by the tensile testing methods, based on the small percent difference. Although it precisely measured the pure control material, the modified tensile test performed may not be appropriate for a composite material or a small layered brittle material as seen with the inability to determine a Young's Modulus from the data for the 0.0 mm and 0.4 mm specimen.

A hypothesized explanation for the results is that the laser extensometer was not precise enough to capture extension data, thus causing repetition of strain values (Appendix B). Furthermore, as mentioned in section 1.4.2, the modified ASTM D638-10 standard used to create the tensile specimen may also contribute to the inability for proper collection of data.

Considering the entire specimen geometry for tensile testing, only a small portion of the gage length was made of the piezoelectric composite material of interest. Meanwhile, the ASTM standard assumes that the entire specimen created, is a single material that represents the bulk material. However, because it was not a full composite specimen, the overall geometry of this "modified" tensile testing specimen may not conform to the standards requirements, and therefore may not represent the bulk material that is usually assumed when using the standard.[40] Thus, using tensile testing and applying the parameters required by the test may not be appropriate for this specimen type (i.e. rate of testing). With such a small portion of the specimen being the

composite insert, bulk features may not be accounted for as well when setting the parameters. Whereas if the assumption was valid of a full tensile specimen representing the bulk material, the features may be accounted for when running the test. There is potential that this explains why the data and Young's Modulus could be calculated and obtained from the control samples but not the 0.0 mm and 0.4 mm samples: it is a full tensile specimen made entirely of the cured epoxy material.

Prior to experimentation, it was predicted that there could be early failure of the brittle tensile specimen due to the stress concentrations generated around the thicker brittle ceramic section. Upon close examination of the failed 0.0 mm and 0.4 mm specimens, the failure did occur at one of the interfaces where the composite was attached to the epoxy tabs. It is likely that this failure mode occurred because of both the stress concentration of the ceramic and the weakened bond interface. If the bond had defects or if the specimen was slightly misaligned in the grips, the influence of this defect would be even greater and lead to early failure. In the case of early failure, the data acquisition capabilities of the laser extensometer (0.0001 inch) were not sufficiently sensitive to capture the small deformations that occurred before failure. The control specimens did not experience this issue because the specimen was made of one material and did not contain any interfaces in which improper bonding or additional stress concentrations could have occurred. Because of the early failure and insufficient data resolution of the laser extensometer, the deformation data for the 0.0 mm and 0.4 mm specimen was not appropriate for analysis. The control specimen could be analyzed. From the data of the 0.4 mm and 0.0 mm specimen, failure loads were on average 15.8(8.6) MPa for the 0.0 mm specimen, while failure occurred on average at

16.8(6.2) MPa for the 0.4 mm specimen. The highest average failure load occurred for the control specimen at 164(4.4) MPa. It would be expected that the higher tensile strength and stiffness of the brittle PZT would result in reinforcement of the composite, thus yielding higher composite tensile strength as compared to the neat epoxy control. However, the stress concentrations and subsequent early interface failure also yielded results that did not reflect theoretical behavior.

2.4.2 Additional Tensile Testing Analysis

Theoretical calculations were still made to understand the expected mechanical behavior of the material under uniaxial tensile stress. The theoretical calculations utilized composite theory in which the Rule of Mixtures was used to predict transverse stiffness (Equation 1).

$$E_2 = \frac{E_f E_m}{E_m V_f + E_f\left(1 - V_f\right)} \qquad \text{Equation 1}$$

Calculations can be seen in Appendix C. Based on the results of the theoretical calculations, the stiffness for a 0.0 mm composite material is 78,000 MPa. This is with the assumptions that the addition of the different layers does not contribute to the overall stiffness. The theoretical stiffness for a 0.4 mm composite material is 3,480 MPa. Thus, the addition of compliant layers decreased the stiffness, as predicted. Therefore, had the experiment been successful, this is what would have been expected for the stiffness of the 0.0 mm specimens versus the 0.4 mm specimens. Having a material

with a lower elastic modulus for an interbody implant is desirable because it allows for more deformation without plastically deforming.

2.4.2 Fracture Toughness Analysis

Fracture toughness of a material is helpful in predicting how well a material can resist crack propagation. It was demonstrated that the control specimen's fracture toughness was highest as originally hypothesized. However, the 0.0 mm and 0.4 mm specimens did not have a fracture toughness value as was expected. The 0.4 mm specimen had a lower fracture toughness value than that of the 0.0 mm specimen which is contradictory of the original hypothesis.

Because the analysis revealed results that were unexpected, reexamination of the procedure of specimen fabrication and analysis was made. It was hypothesized that one of the main reasons for the unexpected results is that initial crack through the specimen was not propagated long enough so that it reached into the sample. Slight errors in the dimensions (not exact) could have caused the specimen embedded to be smaller than intended. The possibility that the overall fracture toughness specimen was not sanded down small enough to be precisely 10 mm in height may have also contributed to the error in crack length. Additionally, because the initial crack followed initial crack length boundaries mentioned in section 2.2.3, following just the standard limitations may have elicited a crack that was not long enough to have reached into the actual material to be tested when remaining in bounds. Examination of crack initiation images of 0.0 mm and 0.4 mm specimen revealed a majority, if not all, of the specimens did not have a crack that reached into the material of interest (Figure 29-38). The space

of epoxy between the crack tip and specimen material ranged from 0 mm to 0.4 mm (a whole PZT disc thickness)

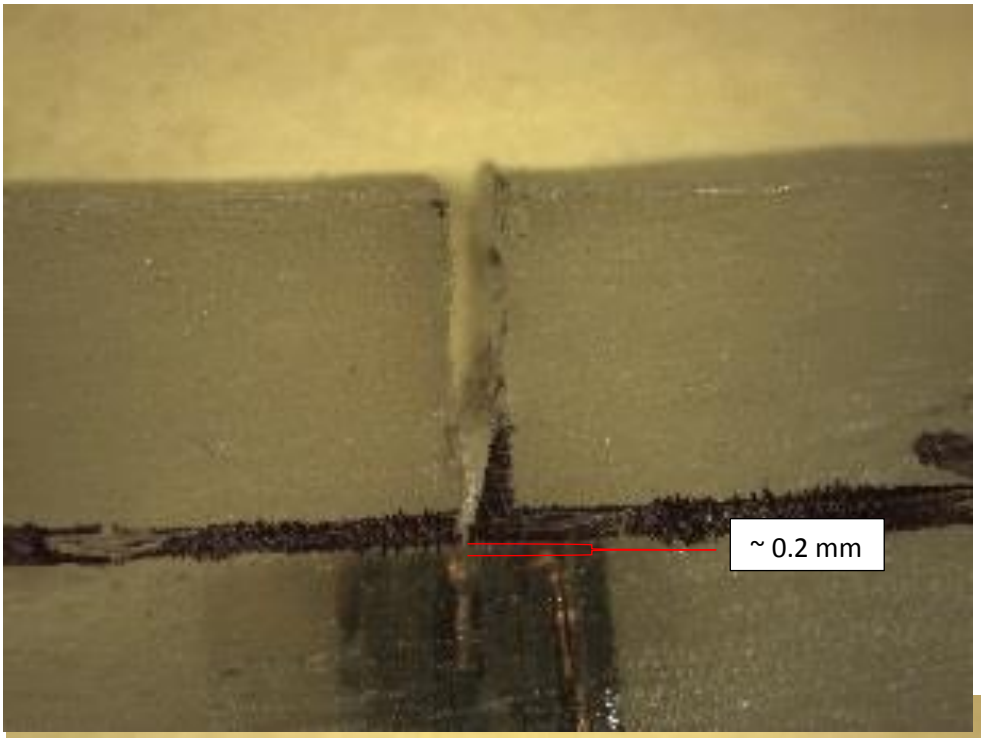

Figure 29: Image of 0.0 mm specimen #2; indicating space between crack tip to 0.0 mm material for fracture toughness to be ~0.2 mm.

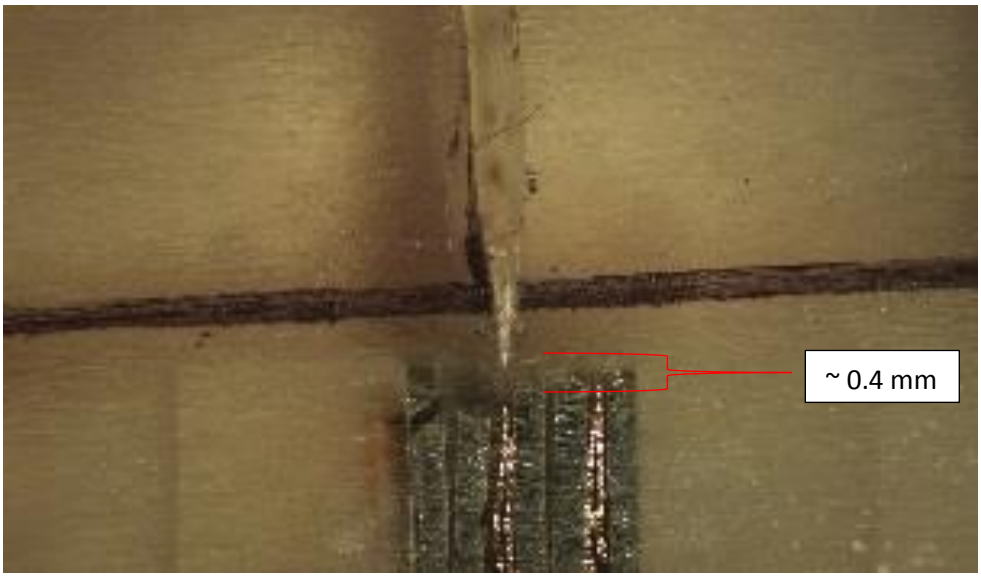

Figure 30: Image of 0.0 mm specimen # 1; indicating space between crack tip to 0.0 mm material for fracture toughness to be about 0.4 mm.

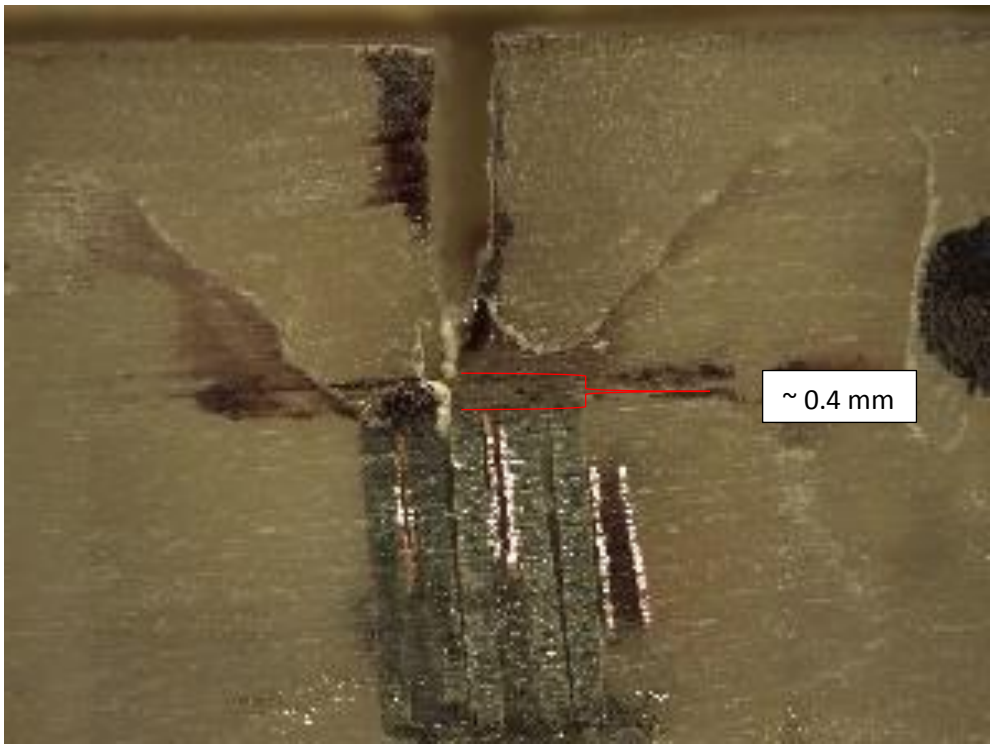

Figure 31: Image of 0.0 mm specimen #3; indicating space between crack tip to 0.0 mm material for fracture toughness to be ~0.4 mm.

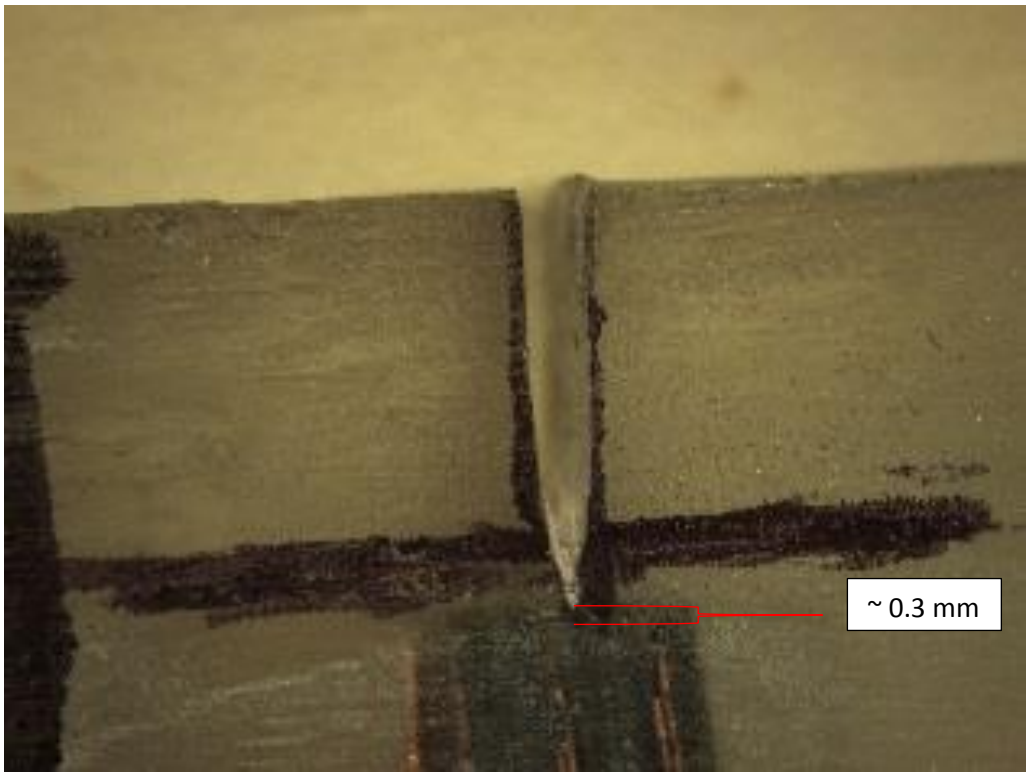

Figure 32: Image of 0.0 mm specimen #4; indicating space between crack tip to the 0.0 mm material for fracture toughness to be ~0.3 mm.

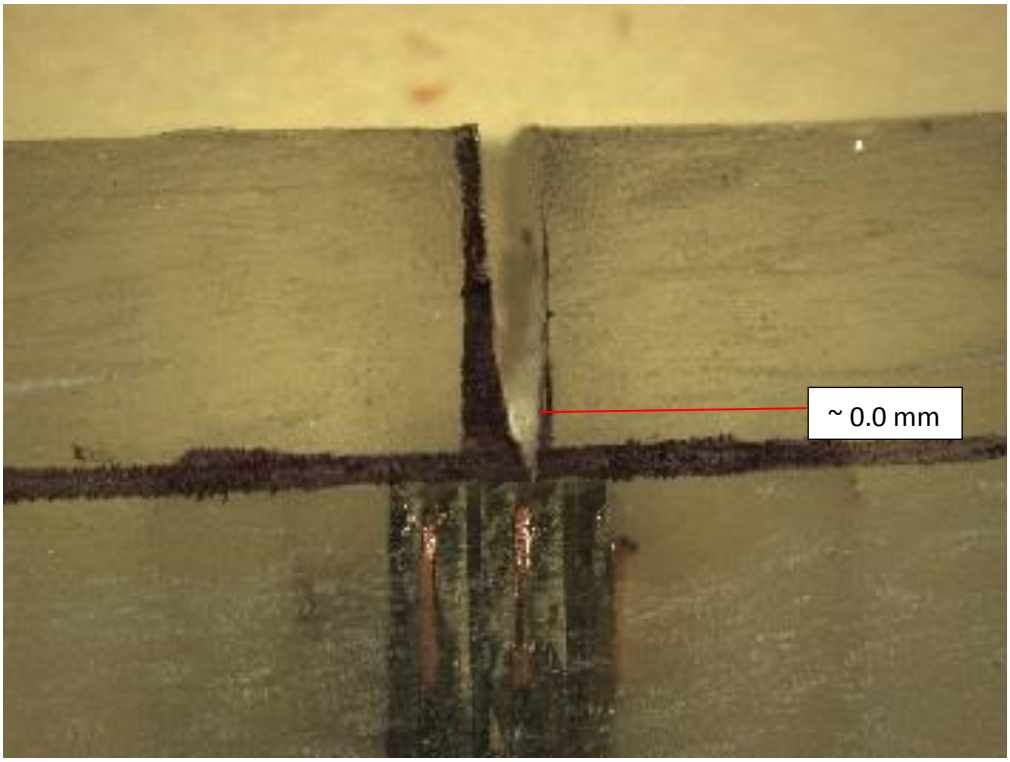

Figure 33: Image of 0.0 mm specimen #5; indicating space between crack tip to the 0.0 mm material for fracture toughness to be ~0.0 mm.

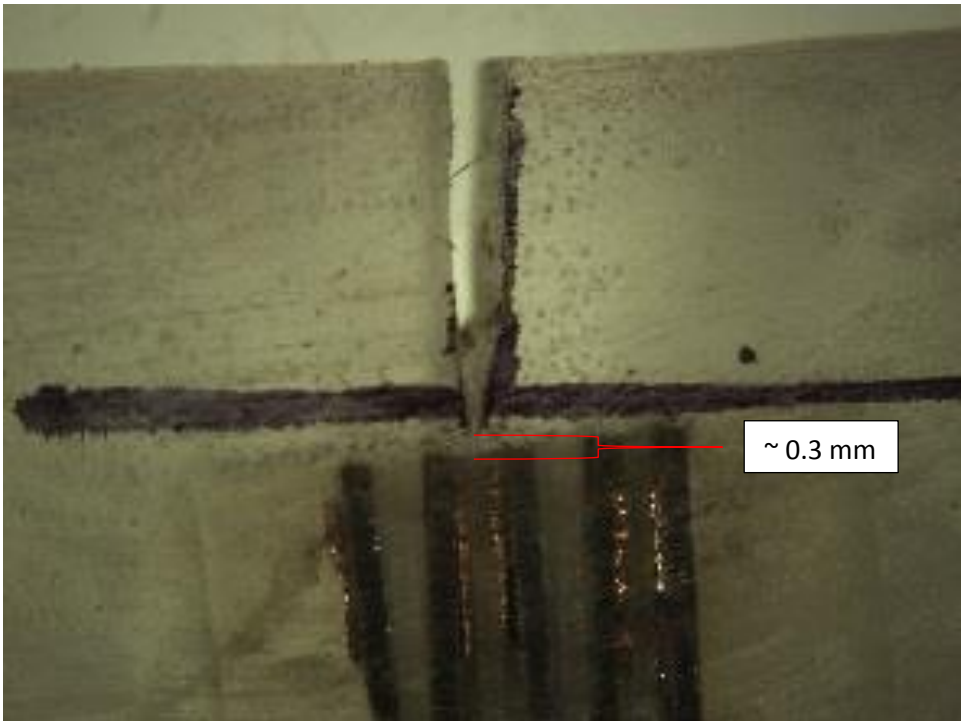

Figure 34: Image of 0.4 mm specimen #1; indicating space between crack tip to the 0.4 mm material for fracture toughness to be ~0.3 mm.

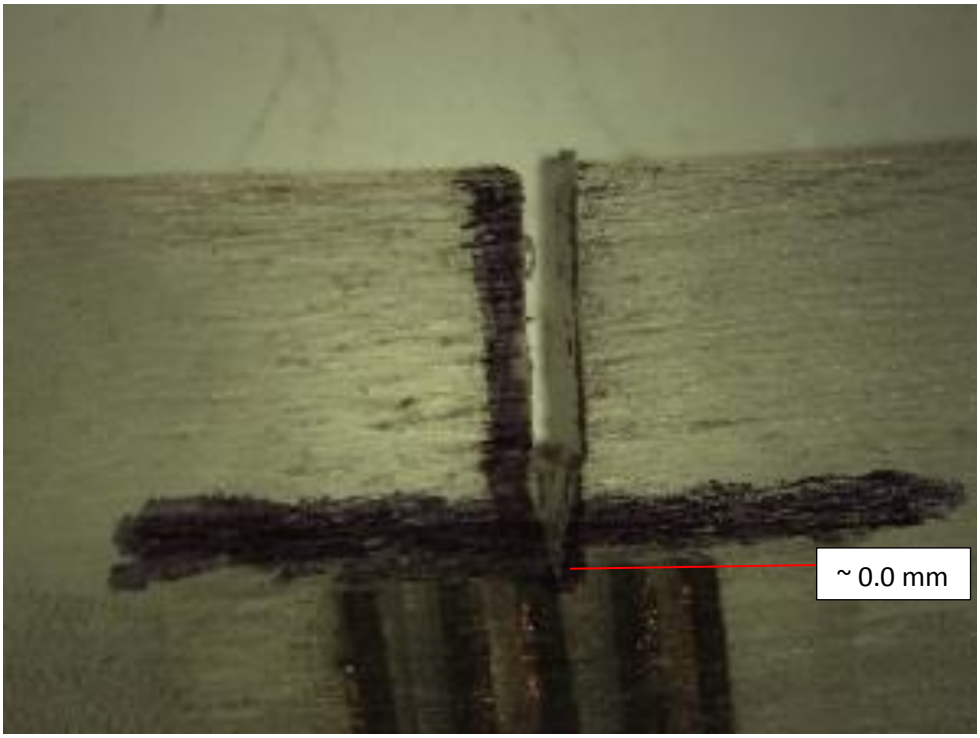

Figure 35: Image of 0.4 mm specimen #2; indicating space between crack tip to the 0.4 mm material for fracture toughness to be ~0.0 mm.

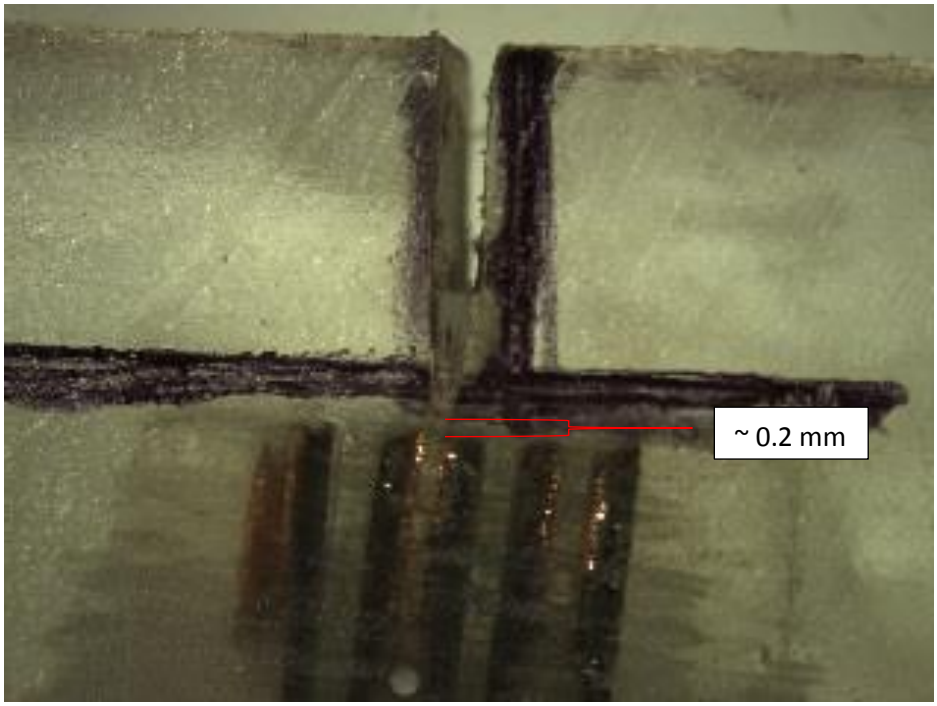

Figure 36: Image of 0.4 mm specimen #3; indicating space between crack tip to the 0.4 mm material for fracture toughness to be ~0.2 mm.

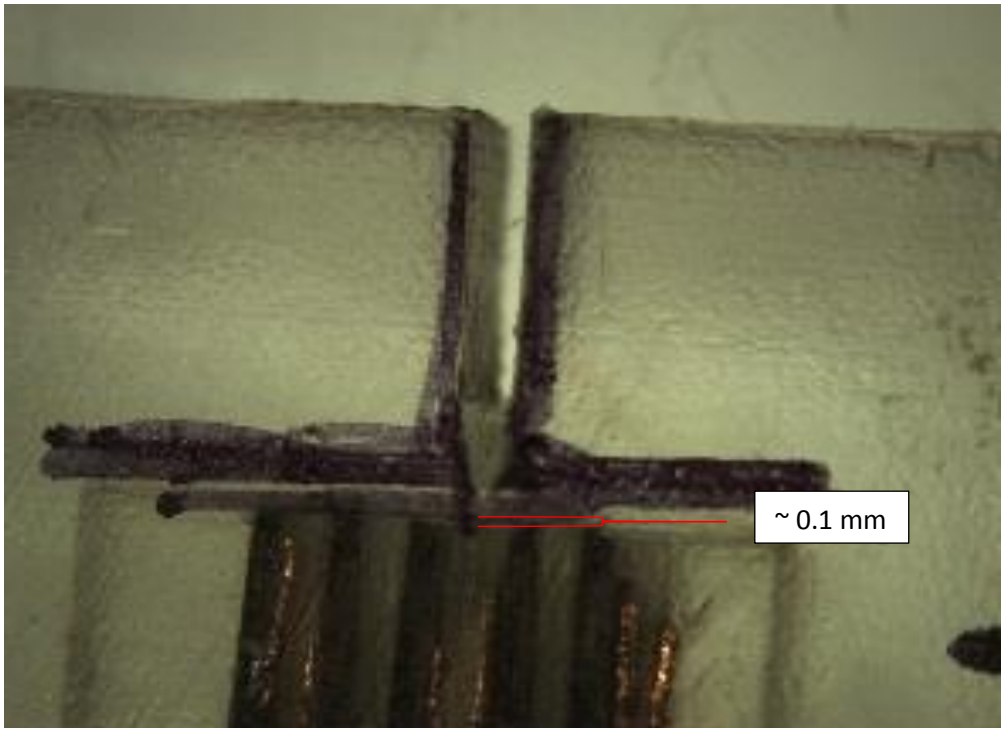

Figure 37: Image of 0.4 mm specimen #4; indicating space between crack tip to the 0.4 mm material for fracture toughness to be ~0.1 mm.

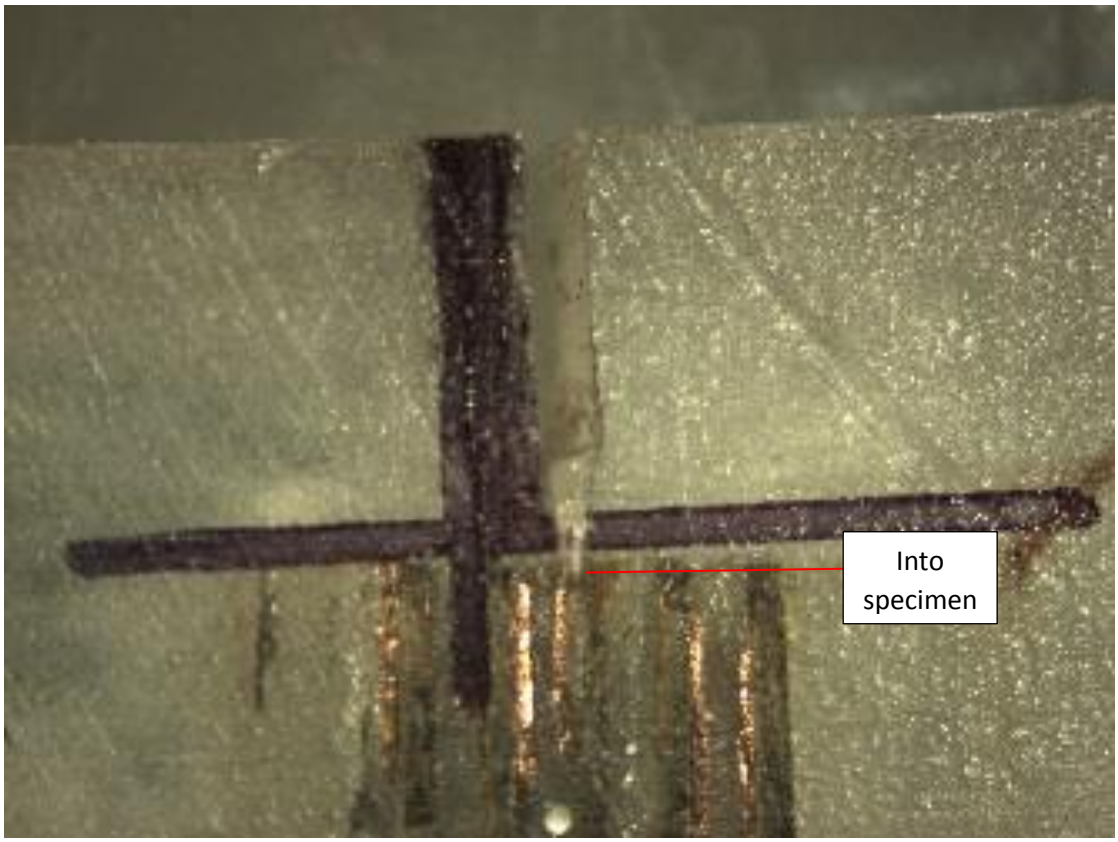

Figure 38: Image of 0.4 mm specimen #5; indicating space between crack tip to the 0.4 mm material for fracture toughness was none since the crack went into the specimen.

Because the crack tip did not reach into the specimen for all but one sample tested, the fracture toughness data would have captured not only the material of interest, but the excess epoxy that surrounds the composite material. Therefore, the fracture toughness value would be higher than originally expected. This is especially true for the 0.0 mm layer, since it is expected to have a lower fracture toughness, but it ended up having a higher fracture toughness value. The fracture toughness value has dependency on how much epoxy was above the material of interest where the crack had to propagate through during testing. Because the crack was not long enough, it was observed the 0.0 mm and the 0.4 mm results were unreliable. Therefore, the statistical analysis presented previously is meaningless.

Due to electrical connection of the discs, there was a thin layer of copper foil present around the area of the initial crack. Thus, it was also hypothesized that the additional materials within the layers of both specimen could have contributed to energy absorption. The results may reflect the additional material properties as well, and not just the composite material properties of interest. Further analysis and experimentation was performed to investigate this phenomenon.

2.4.3 Additional Fracture Toughness Testing & Analysis

Theoretical calculations of the crack tip plastic zone were performed with consideration of the experimental specimen and materials present in the layers of the 0.0 mm and 0.4 mm specimen. The crack tip plastic zone is defined as the area in front of the crack tip in which plastic deformation of the material occurs.[42] In this region, the energy absorption of the crack is dependent on the material within this region. This condition helps determine whether crack growth can occur or not, which is again

dependent on the material in front of the crack tip, or the crack tip plastic zone.[42]

Equation 2 was used for the calculation of the radius of this crack tip plastic zone:

$$r_y = \frac{1}{2\pi}\left(\frac{K_{IC}}{\sigma_{ys}}\right)^2$$

Using Eq. 2, the radius of the plastic zone contributed by the epoxy, the PZT discs, and the copper foil was determined using known yield strength values (σ_{ys}) and control samples (Table 2). It was assumed that the small amounts of conductive epoxy were negligible.

Table 5: Comparison of the radius of the plastic zone for each present material in the 0.0 mm and 0.4 mm fracture toughness specimen, assuming just purely the material listed.

	K_{IC} (MPa·m$^{1/2}$)	Yield Stress (MPa)	r_y (mm)	Experimental Layer Thickness (mm)
Ceramic (min, max)	0.50 [A]- 0.90	83 [B]	0.01-0.02	0.40
Epoxy (experimental)	3.35	32.29	1.71	0.40
Copper Foil	26 [C]	110 [D]	8.89	0.05

[A] M. F. Ashby - Materials Selection in Mechanical Design, Pergamon Press, Oxford, 1992.
[B] matweb.com
[C] www.nickel-alloys.net/copper_nickel_alloys.html
[D] https://www.copper.org/publications/pub_list/pdf/a1360.pdf

From the theoretical analysis, copper foil was found to have the largest radius of the plastic zone in front of the crack tip (Table 2). Meanwhile, the ceramic discs have the smallest radius. This analysis showed that if the crack tip were to encounter the PZT ceramic, it would absorb less energy than compared to the copper foil. Although the copper foil's thickness is smaller than that of the ceramic, if the crack tip encounters

copper foil first, than most of the energy absorption will be absorbed by the copper and not the PZT ceramic. Thus, the overall fracture toughness of the specimen value would reflect the copper foil properties, as opposed to the other materials present.

Reviewing the theoretical results, the trend seen in the original results of fracture toughness is not what should have happened in the experimental study. Addition of the compliant layers of epoxy should have contributed higher energy absorption than the 0.0 mm specimens made of ceramic alone. Therefore, not only are the results invalid due to the improper crack initiation, but if the crack was formed at an interface in which it would have encountered copper, it may have skewed the results as well. This is highly likely because the placement of the copper foil strips to connect the discs are present in between every layer of material once folded to stack the discs.

To determine if the copper foil contributed a high amount of energy absorption, a second crude experiment was performed. This experiment involved manufacturing two insert types with no conductive epoxy present, or copper foil (n = 1, 0.0 mm; n = 1, 0.4 mm). These specimens were then embedded like the original specimens for fracture toughness, and the crack clearly engaged with the composite material (Figure 39). With proper crack initiation into the specimens, concern for capturing excess epoxy along with the composite material of interest was eliminated from these results. These specimens were fabricated identically to the dimensions used in the original specimen, and then tested using a three-point bend test. The results can be seen in Figure 40.

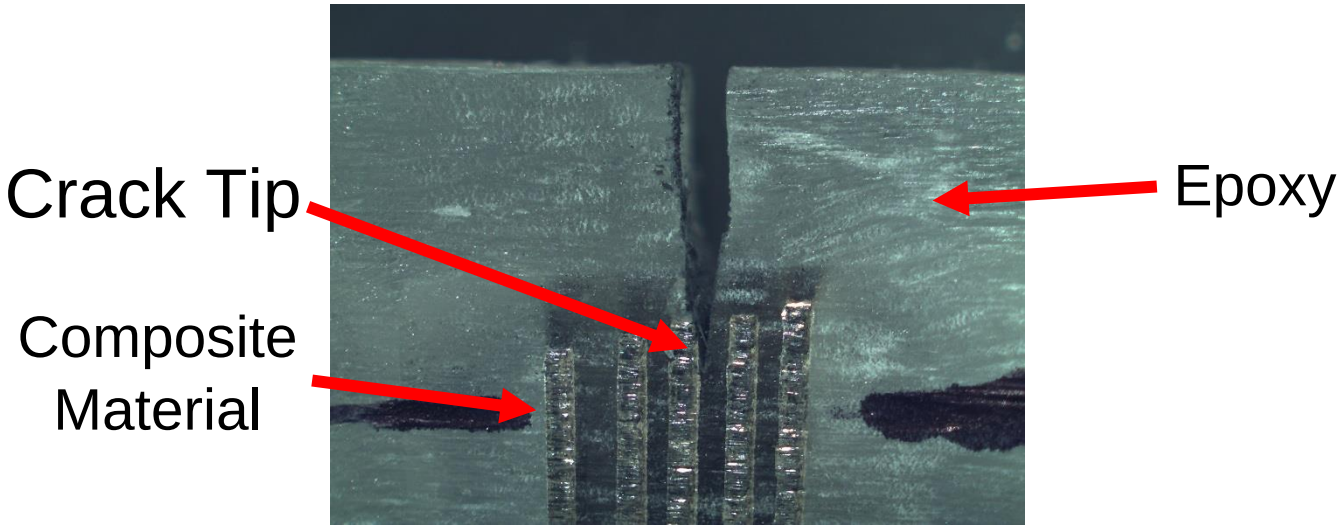

Figure 39: Image of a 0.4 mm layer specimen with no copper foil or conductive epoxy with a proper crack initiated into the composite material.

Without conductive epoxy or copper foil in between the layers of the one specimen tested, and a correct crack initiated, the one 0.0 mm fracture toughness specimen yielded a fracture toughness value that was almost 50% smaller than that of

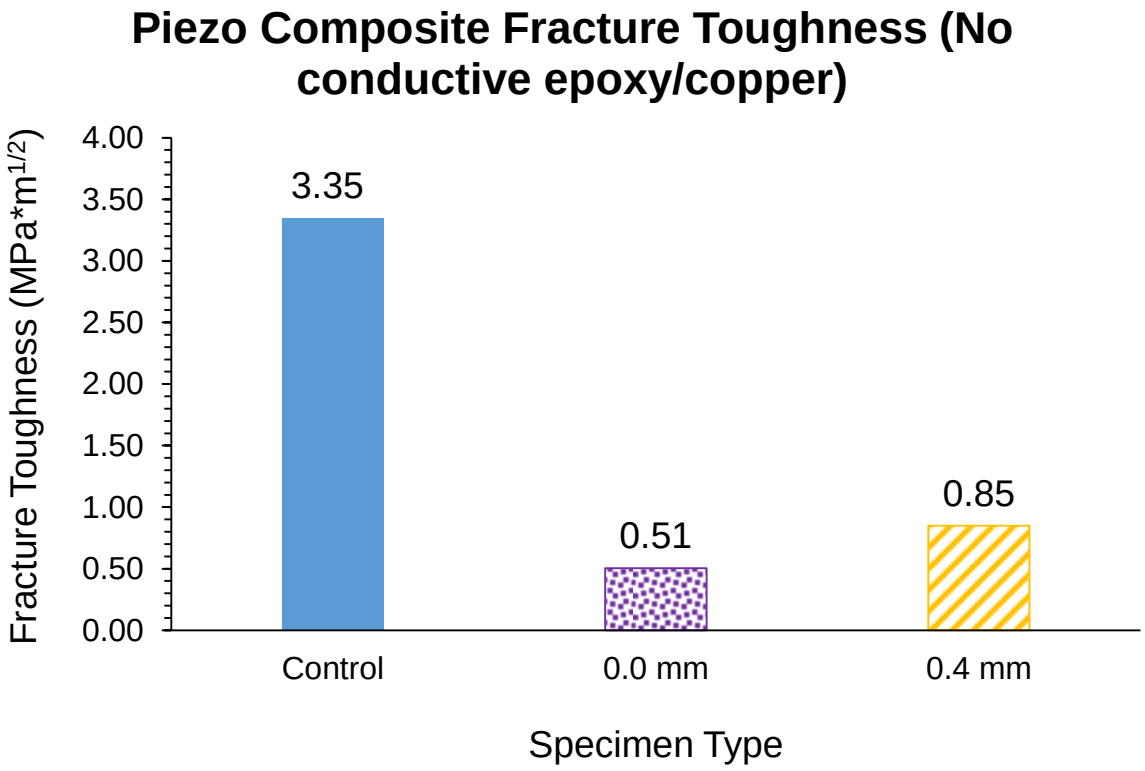

Figure 40: Comparison of additional fracture toughness values for each specimen type, made without conductive epoxy and copper strips. Note that the 0.0 mm specimen type is purely stacked discs, and the 0.4 mm specimen type is purely stacked discs with compliant layers

the 0.4 mm specimen. Although, n = 1 for this experiment, it was a preliminary and crude experiment to determine potential effects of the crack tip encountering the copper foil first, as well as determining how the incorrect crack tip, when correctly done, can influence the final results.

Relating these experimental results back to the theoretical calculations, the trend seen, is what may have been if crack tip initiation was performed properly and no copper foil was present. With the absence of copper foil, a crack initiated properly into the 0.4 mm fracture toughness specimen, would have elicited an area in front of the crack tip that is mostly contributed by the epoxy layer (Figure 41). This phenomenon however, would also be present in the 0.0 mm fracture toughness specimen, as they too originally had copper foil within them. The only difference is that the 0.0 mm specimen would have a crack tip that is skewed largely towards a brittle layer since there are no compliant layers present, resulting in a lower fracture toughness value as seen in Figure 43. Considering the layer thicknesses of the PZT layer and the epoxy compliant layer were the same, and the maximum and minimum of the radius, calculated in Table 2**,** for both material layers, the radius in front of the crack tip would be much larger for the epoxy layer as compared to the PZT layer. Again, considering Table 2, the calculations explain why the control samples of epoxy demonstrated the highest value of fracture toughness. This is due to the large radius that is present in the pure epoxy when crack is initiated. In a pure epoxy sample, it has no interface or brittle material presence leading to a larger area of energy absorption especially with the large crack tip energy field present (Figure 42).

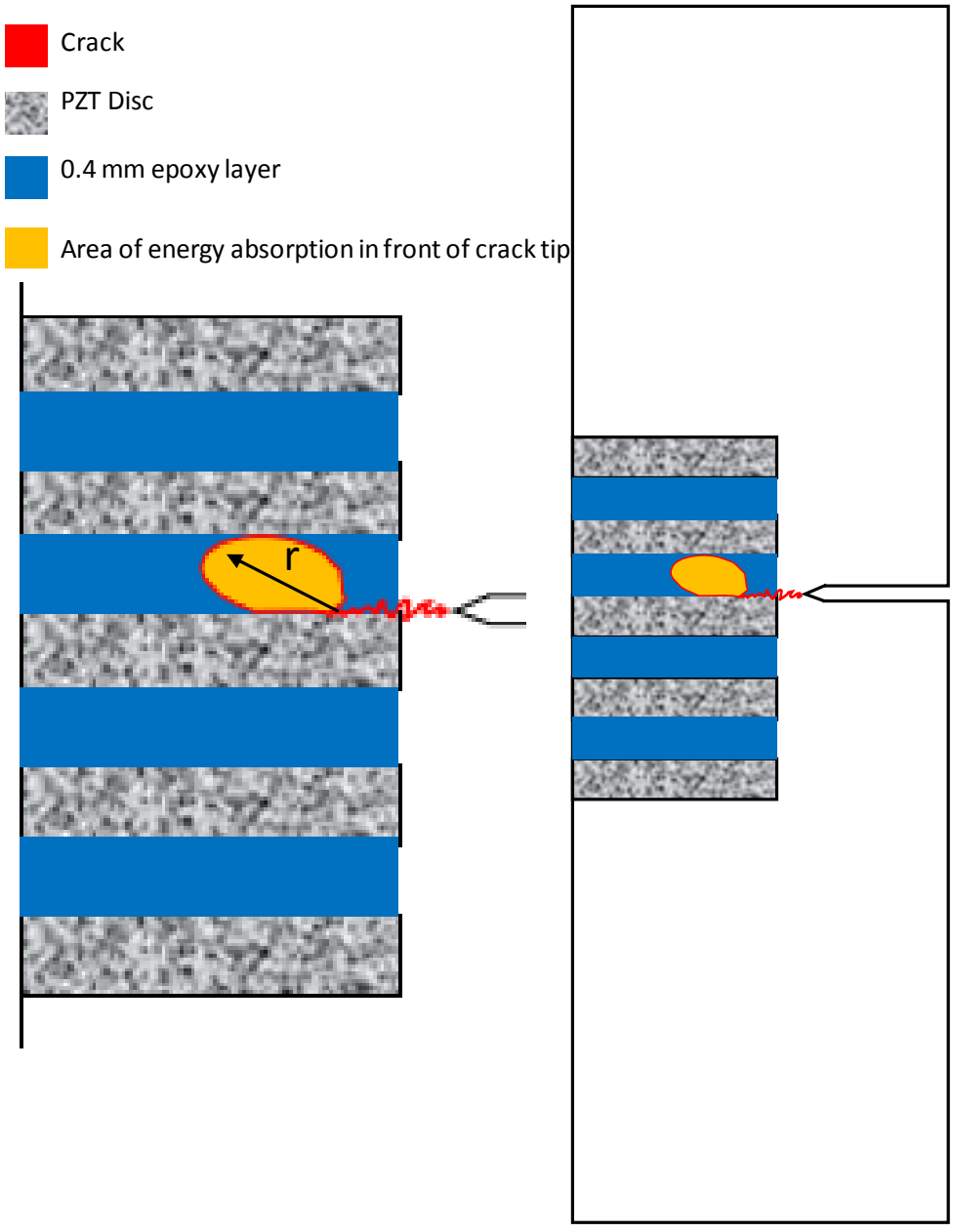

Figure 41: A theoretical/predicted schematic magnified of the 0.4 mm fracture toughness specimen with no conductive epoxy or copper a crack initiated into the material of interest to reveal the area of energy absorption in front of the crack tip. This radius is two magnitudes higher than the 0.0 mm material; r = 1.71 mm.

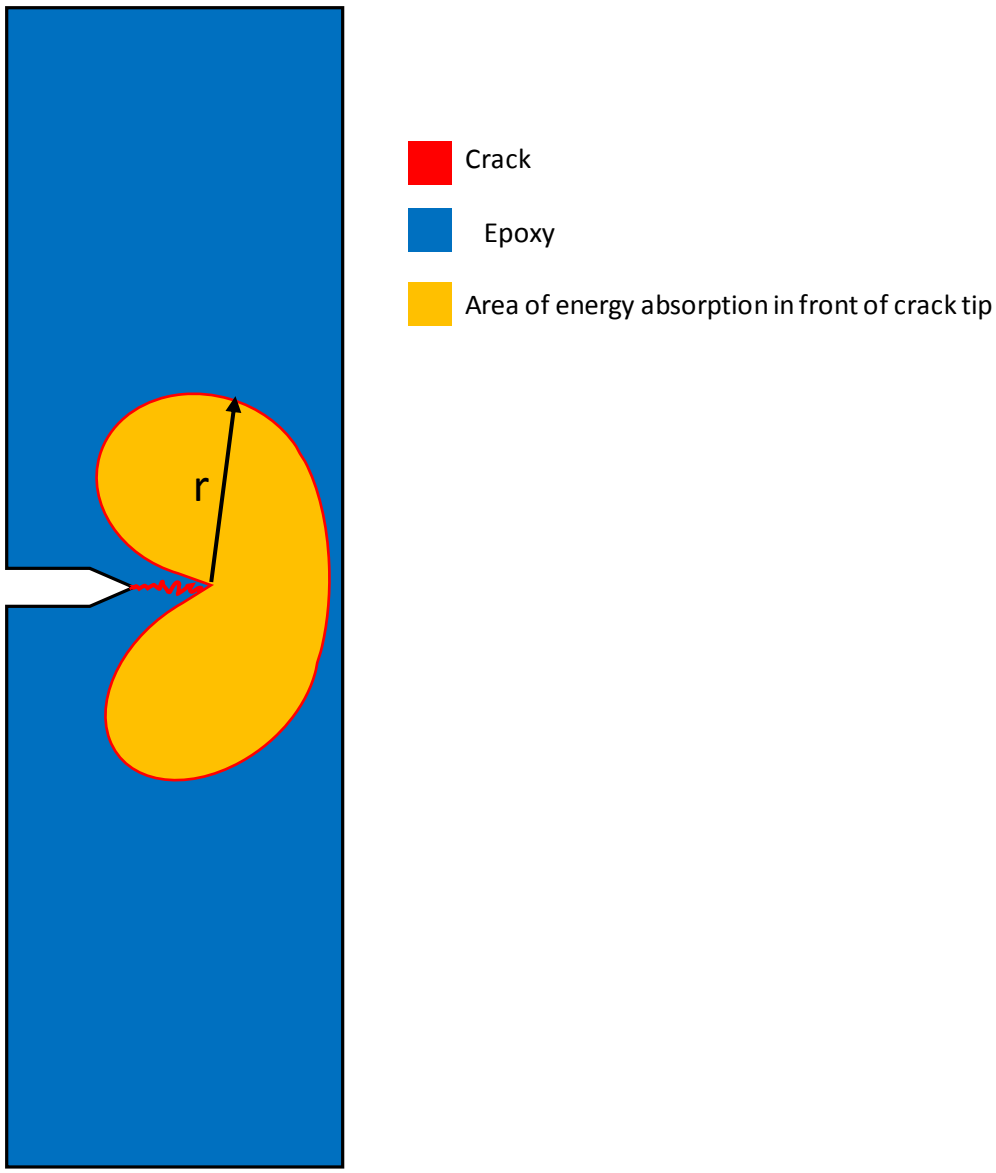

Figure 42: A theoretical/predicted schematic magnified of epoxy control fracture toughness specimen with no other materials with a crack initiated to reveal the area of energy absorption in front of the crack tip. The radius of the crack tip energy field large because it is all epoxy in front of the crack tip which can absorb a large

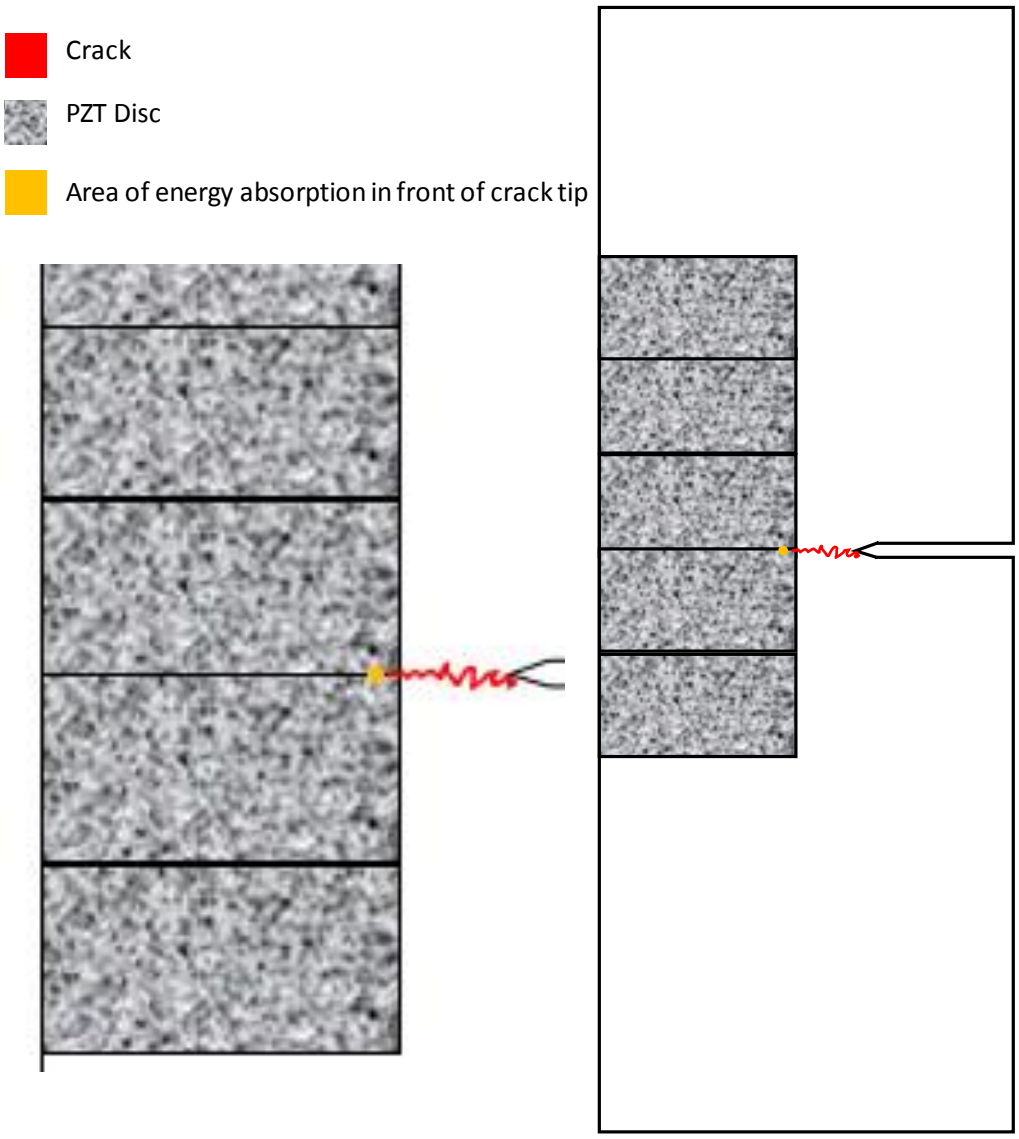

Figure 43: Theoretical/predicted schematic magnified of a 0.0 mm fracture toughness specimen with no conductive epoxy or copper with a crack initiated to reveal the area of energy absorption in front of the crack tip. The radius of the crack tip energy field is the same around the crack tip because both materials around the crack is the same. This radius is two magnitudes smaller than with intermediate epoxy layers; r = 0.01 to 0.02 mm.

Examining the 0.0 mm fracture toughness specimen, the crack tip would have encountered only PZT material in front of the crack tip, therefore the area in front of the crack tip that absorbs energy would be evenly distributed due to the same material being encountered on either side of the layer interface (Figure 43). Because the energy is not absorbed as much with layers of PZT on both sides of the crack tip, the crack would propagate into the interface early on because it is assumed that the material's interface is its weakest point. However, with all layer thicknesses the same, with the contribution of a compliant layer and its larger radius of plastic zone in front of the crack tip, the theory expresses that the 0.4 mm fracture toughness specimen should have higher fracture toughness. Ultimately, this is due to the ability of the larger radius of plastic zone to absorb more of the energy produced by the crack tip, compared to the smaller radius of the plastic zone of the PZT layer. Because the radius of the crack tip energy zone is over two magnitudes larger than the PZT's radius, the crack has a much lower ability to propagate down the interface as the epoxy layer absorbs much of the energy. This demonstrates that a material exhibiting a higher fracture toughness value is valuable when considering what material to use in designing a spinal fusion implant. Because the addition of compliant layers can increase the fracture toughness, the 0.4 mm composite material could help prevent the implant from failing catastrophically due to crack propagation induced during loading of the spine.

2.5 Conclusion

With tensile testing of the 0.0 mm and 0.4 mm specimen, there was an inability to conclude elastic modulus information from the results due to the insensitivity of the equipment available. Additionally, specimen fabrication was not ideal due to the limited

materials available. Fracture toughness testing yielded results that contradicted the original hypothesis formed, however, with a second look from a theoretical point of view, it is evident that the addition of copper foil may have skewed the results. This is also true of the improper initiation of the crack. Therefore, with the theoretical calculations, and the results of the crude experiment, it is highly likely that the 0.4 mm specimen should have had a higher fracture toughness value than that of the 0.0 mm. Overall, testing was important because it demonstrated that the specimen need to be properly prepared to acquire accurate data. This is especially important when testing materials for implants because if the material properties are not accurate, it puts the patient at risk if the implant were to fail sooner than expected. Ultimately, materials that exhibit a higher fracture toughness, as is expected with the 0.4 mm composite, are valuable for maintaining the integrity of a spinal fusion implant.

Chapter 3: Summary

3.1 Conclusions & Recommendations

The study performed was to investigate the integrity of a novel composite that has potential for use in a spinal fusion implant. The study examined three material types, a control made of epoxy, a 0.0 mm PZT stacked material, and a 0.4 mm PZT stacked layer that included compliant layers. To test the integrity and compare each of the materials, uniaxial tensile testing, and plane-strain fracture toughness tests were used to evaluate these materials. Overall, uniaxial tensile tests for polymers were an appropriate test to run on the control epoxy samples, as was described in the discussion, since the sample average value was less than 1% different than the published theoretical value. However, when considering the 0.0 mm composite material and the 0.4 mm composite material, erroneous data collected revealed that the Young's modulus could not be determined using the equipment available. Early failure of the material due to a potentially weak interface between the epoxy tabs and the material of interest, and the lack of precision of the laser extensometer was the cause of the inability to calculate the modulus. However, failure loads were consistent with what was predicted as the 0.4 mm specimen required a higher load to fail than that of the 0.0 mm specimen.

Recommendations for improvement for the tensile testing include developing specimen that are purely made from the composite material or purely out of the PZT discs. By developing samples without the epoxy tabs, it will eliminate the possibility that there was a poorly bonded interface between the epoxy tabs and the material of interest

that may have caused the premature failure. Thus, failure of the specimen would not be caused by interfacial bonding, but rather the composite material itself. The experimental construct needs to be improved so that bonding is insured to be fully bonded between the tabs and the composite material, or the whole specimen needs to be made of the composite to prevent the premature failure.

Another improvement includes developing tensile specimen the same way as originally done in the study, but instead, prior to testing, notches will be made to ensure that the material attached to the dog bone tabs are more narrow. By including this notching method, the break is controlled and isolated within the boundaries of the narrow region in which the entire dog bone is notched. To prevent premature breaking, these notches would be made after the interface at which the tabs are bonded to the material.This will prevent influence of the poorly bonded interface.

Additionally, it was found that fracture toughness testing with a composite material and the modifications made to the ASTM standard, requires careful attention when fabricating specimen. Fracture toughness values were considered not valid because the initiated crack during specimen fabrication did not reach into the specimen and therefore the results could have captured load vs displacement data of the epoxy prior to the embedded material. However, with theoretical calculations to determine the radius at the front of the crack type, there was revelation of the expected trend for toughness. Specifically, the results should have revealed that the 0.0 mm material should have had a lower toughness than that of the 0.4 mm material, and therefore should be significantly different. Ultimately, the theory and crude experiment performed revealed that it can be concluded that the addition of compliant layers to the PZT discs

allow for an overall tougher material, and thus should also be exhibited in the experimental study.

Recommendation for the future would include a full experiment to determine fracture toughness, but with 0.0 mm and 0.4 mm specimen not including any materials that would not be present in the final manufactured implant. There also needs to be further investigation into separating the effect of proper crack initiation and the addition of the copper foil within the material. Although theoretical results revealed that fracture toughness should have been higher with the compliant layers, the true experimental effect of the copper is still unknown. Therefore, it would be necessary to conduct more studies in separating the two potential effects on the fracture toughness of the composite material. Improper and proper crack initiation should be compared, while eliminating copper and keeping copper within the sample should be compared. Once these are investigated, combinations of both should also be tested to determine their true effects.

3.2 Study Limitations

It is important to understand that throughout the process of the study, there were several evident limitations. It was not realistic to make large sample sizes, as well as, develop fracture toughness and tensile specimen fully out of the PZT material as there were only five specimen of each 0.0 mm specimen type and 0.4 mm specimen type that could be used for tensile and fracture toughness testing. Therefore, the ASTM standards were modified to allow for more realistic specimen. The sample size used for each specimen type may have also been a limitation because n = 5 may not have been a representative size. Because it was a small sample size, a Type II error could have

occurred and created overlapping standard error, therefore significant difference between the types of specimen may be a false negative.

It was also unrealistic to purchase additional and larger discs to develop a tensile or fracture toughness specimen made entirely of the two materials. This is because there was a large limitation on time, in which the materials took up cost in terms of the time to purchase to the time received. Therefore, the tensile specimens, as well as, the fracture toughness specimens were largely made up of the epoxy (attached epoxy tabs), as opposed to the materials of interest, as time could not be spent purely waiting for specimen arrival. With larger orders of PZT discs, the more time it would take for them to be manufactured and delivered. Additionally, the amount necessary may also not have been in stock when needed as the distributer only had a limited supply.

The equipment used to perform the study also had its own limitations. Assumptions were made that the rollers were small enough to have a point contact, however, considering how small the specimen size of interest is compared to the epoxy of the test sample, it may have been a large enough point that it did not reflect the bulk material of the 0.0 mm and 0.4 mm material during testing.

The repeating extension values during tensile testing also revealed that the equipment available was not precise enough in measuring displacement. The small displacement ultimately could not be detected to a precise decimal. The laser extensometer did not have the capability in detecting the small changes in displacement in between successive points, and thus the values seemed to have repeated themselves.

There was also a limitation in manufacturing due to the specimen size. It was difficult to handle such small materials with precision and accuracy during fabrication with the limited equipment available. Mistakes during fabrication is highly inevitable because it was fabricated by hand as opposed to contracting out where the specimen could be produced using machinery capable of high precision and accuracy. Under all the above circumstances, the limitations have a large contribution to the unsuccessful testing of the composite specimens.

3.3 Future Work

Future work of this study includes testing a much larger sample size given a limitation on fabrication steps, and equipment. With a larger sample size, variation that may be prominent in a smaller sample size, may not have as large of an effect due to the ability of a larger sample size to represent a population. Sample size ideally should be changed to n = 20 in future work to repeat this study.

Because the tensile specimen had early failure, future work should include tensile specimen fully out of the PZT material of interest. If this is not possible, there is the possibility to rerun a test where the tensile specimen contained a notch. From notch tensile testing, a notched tensile strength can be determined which is analogous to ultimate tensile strength. During a notch test, there would be a reduction in the section size at the location of the composite material. With a reduction in size, higher stress concentrations would be created away from the composite connection site to the epoxy tabs. However, it is important to keep in mind that this methodology may still not overcome the early failure. Thus, this methodology would require a combination of a

notched tensile specimen and a tensile specimen made entirely of the composite material.

There could also be substantial work done in examining the theory mentioned previously using Finite Element Modeling (FEA) with the appropriate assumptions. FEA can uphold an ideal and controlled test, which can eliminate the variants that could affect the results of the data. Therefore, with an FEA study, it may be beneficial to compare its results to the theoretical calculations, as well as, a future re-run of the entire study to better understand the mechanics of the material undergoing stress with or without compliant layers.

References

1. Brantigan JW, Steffee AD. A Carbon Fiber Implant to Aid Interbody Lumbar Fusion: Two-Year Clinical Results in the First 26 Patients. Spine. 1993;18:2106.

2. Hirsch C. The reaction of intervertebral discs to compression forces. J Bone Joint Surg Am. 1955;37–A:1188–96.

3. Inoue N, Espinoza Orías AA. Biomechanics of Intervertebral Disc Degeneration. Orthop Clin North Am. 2011;42:487–99.

4. Rajaee SS, Bae HW, Kanim LEA, Delamarter RB. Spinal Fusion in the United States: Analysis of Trends From 1998 to 2008. Spine. 2012;37:67–76.

5. Gallinaro P, Indemini E, Tabasso G, Abbate M. Spinal fusion in degenerative disc disease. Chir Organi Mov. 1994;79:101–5.

6. Djurasovic M, Glassman SD, Dimar JR, Howard JM, Bratcher KR, Carreon LY. Does Fusion Status Correlate with Patient Outcomes in Lumbar Spinal Fusion?: Spine. 2011;36:404–9.

7. Kumar MN, Jacquot F, Hall H. Long-term follow-up of functional outcomes and radiographic changes at adjacent levels following lumbar spine fusion for degenerative disc disease. Eur Spine J. 2001;10:309–13.

8. M Phillips F, Slosar P, Youssef J, Andersson G. Lumbar Spine Fusion for Chronic Low Back Pain Due to Degenerative Disc Disease. Jan 17, 2013.

9. Toth JM, Seim HB, Schwardt JD, Humphrey WB, Wallskog JA, Turner AS. Direct current electrical stimulation increases the fusion rate of spinal fusion cages. Spine. 2000;25:2580–7.

10. Meril AJ. Direct Current Stimulation of Allograft in Anterior and Posterior Lumbar Interbody Fusions. Spine. 1994;19:2393.

11. Olsen MA, Mayfield J, Lauryssen C, Polish LB, Jones M, Vest J, Fraser VJ. Risk factors for surgical site infection in spinal surgery. J Neurosurg. 2003;98:149–55.

12. Ho C, Sucato DJ, Richards BS. Risk factors for the development of delayed infections following posterior spinal fusion and instrumentation in adolescent idiopathic scoliosis patients. Spine. 2007;32:2272–7.

13. Olsen MA, Nepple JJ, Riew KD, Lenke LG, Bridwell KH, Mayfield J, Fraser VJ. Risk factors for surgical site infection following orthopaedic spinal operations. J Bone Joint Surg Am. 2008;90:62–9.

14. Gan JC, Glazer PA. Electrical stimulation therapies for spinal fusions: current concepts. Eur Spine J. 2006;15:1301–11.

15. Rogozinski A, Rogozinski C. Efficacy of Implanted Bone Growth Stimulation in Instrumented Lumbosacral Spinal Fusion. Spine. 1996;21:2479.

16. Glazer PA, Glazer LC. Electricity: the history and science of bone growth stimulation for spinal fusion. Orthop J Harvard Med School Online 2002; 4:63-67.

17. Fukada E, Yasuda I. On the Piezoelectric Effect of Bone. J Phys Soc Jpn. 1957;12:1158–62.

18. Griffin M, Bayat A. Electrical Stimulation in Bone Healing: Critical Analysis by Evaluating Levels of Evidence. Eplasty [Internet]. 2011 [cited 2017 Dec 7];11. Available from: https://www.ncbi.nlm.nih.gov/pmc/articles/PMC3145421/

19. Zhuang H, Wang W, Seldes RM, Tahernia AD, Fan H, Brighton CT. Electrical Stimulation Induces the Level of TGF-β1 mRNA in Osteoblastic Cells by a Mechanism Involving Calcium/Calmodulin Pathway. Biochem Biophys Res Commun. 1997;237:225–9.

20. Hartig M, Joos U, Wiesmann H. Capacitively coupled electric fields accelerate proliferation of osteoblast-like primary cells and increase bone extracellular matrix formation in vitro. Eur Biophys J EBJ Heidelb. 2000;29:499–506.

21. Fredericks DC, Smucker J, Petersen EB, Bobst JA, Gan JC, Simon BJ, Glazer P. Effects of Direct Current Electrical Stimulation on Gene Expression of Osteopromotive Factors in a Posterolateral Spinal Fusion Model: Spine. 2007;32:174–81.

22. Gan J, Fredericks D, A Glazer P. Direct current and capacitive coupling electrical stimulation upregulates osteopromotive factors for spinal fusions. Jan 1, 2005.

23. Wang Q, Zhong S, Ouyang J, Jiang L, Zhang Z, Xie Y, Luo S. Osteogenesis of electrically stimulated bone cells mediated in part by calcium ions. Clin Orthop. 1998;259–68.

24. Fredericks D, Petersen E, Bobst J, Glazer P, Nepola J, Simon B. 48. Effects of direct current electrical stimulation on expression of BMP 2, 4, 6, 7, bFGF, VEGF, TGF-β, ALK2 and ALK3 in a rabbit posterolateral spine fusion model. Spine J. 2003;3:89.

25. Kane WJ. Direct current electrical bone growth stimulation for spinal fusion. Spine. 1988;13:363–5.

26. Tejano NA, Puno R, Ignacio JMF. The Use of Implantable Direct Current Stimulation in Multilevel Spinal Fusion Without Instrumentation: A Prospective Clinical and Radiographic Evaluation With Long-Term Follow-Up. Spine. 1996: 21(16):1904-1908.

27. Goetzinger NC, Tobaben EJ, Domann JP, Arnold PM, Friis EA. Composite piezoelectric spinal fusion implant: Effects of stacked generators. J Biomed Mater Res B Appl Biomater. 2016;104:158–64.

28. Aaron RK, Ciombor DM, Simon BJ. Treatment of nonunions with electric and electromagnetic fields. Clin Orthop. 2004;21–9.

29. Cook SD, Patron LP, Christakis PM, Bailey KJ, Banta C, Glazer PA. Direct current stimulation of titanium interbody fusion devices in primates. Spine J. 2004;4:300–11.

30. Kahanovitz N. Electrical stimulation of spinal fusion: a scientific and clinical update. Spine J. 2002;2:145–50.

31. Platt SR, Farritor S, Garvin K, Haider H. The use of piezoelectric ceramics for electric power generation within orthopedic implants. IEEEASME Trans Mechatron. 2005;10:455–61.

32. Platt SR, Farritor S, Haider H. On low-frequency electric power generation with PZT ceramics. IEEEASME Trans Mechatron. 2005;10:240–52.

33. Chen H, Liu M, Jia C, Wang Z. Power harvesting using PZT ceramics embedded in orthopedic implants. IEEE Trans Ultrason Ferroelectr Freq Control. 2009;56:2010–4.

34. Tobaben EJ, Goetzinger NC, Domann JP, Barrett-Gonzalez R, Arnold PM, Friis EA. Stacked macro fiber piezoelectric composite generator for a spinal fusion implant. Smart Mater Struct. 2015;24:017002.

35. Chan SCW, Ferguson SJ, Gantenbein-Ritter B. The effects of dynamic loading on the intervertebral disc. Eur Spine J. 2011;20:1796–812.

36. Azzi VD, Tsai SW. Anisotropic strength of composites. Exp Mech. 1965;5:283–8.

37. Lakes RS. High Damping Composite Materials: Effect of Structural Hierarchy. J Compos Mater. 2002;36:287–97.

38. ASTM D638-10 Standard Test Method for Tensile Properties of Plastics, ASTM International, West Conshohocken, PA, 2010, https://doi.org/10.1520/D0638-10

39. Dent ACE, Bowen CR, Stevens R, Cain MG, Stewart M. Tensile Strength of Active Fibre Composites – Prediction and Measurement. Ferroelectrics. 2008;368:209–15.

40. Kumar K, Pooleery A, Madhusoodanan K, Singh RN, Chakravartty JK, Dutta BK, Sinha RK. Use of Miniature Tensile Specimen for Measurement of Mechanical Properties. Procedia Eng. 2014;86:899–909.

41. ASTM D5045-99 Standard Test Methods for Plane-Strain Fracture Toughness and Strain Energy Release Rate of Plastic Materials, ASTM International, West Conshohocken, PA, 1999, https://doi.org/10.1520/D5045-99

42. Elementary engineering fracture mechanics | D. Broek | Springer [Internet]. [cited 2017 Oct 23]. Available from: http://www.springer.com/us/book/9789024725809

43. Niinomi M. Mechanical properties of biomedical titanium alloys. Mater Sci Eng A. 1998;243:231–6.

44. Launey ME, Ritchie RO. On the Fracture Toughness of Advanced Materials. Adv Mater. 2009;21:2103–10.

45. Bledzki AK, Gassan J. Composites reinforced with cellulose based fibres. Prog Polym Sci. 1999;24:221–74.

46. Thostenson ET, Chou T-W. Aligned multi-walled carbon nanotube-reinforced composites: processing and mechanical characterization. J Phys Appl Phys. 2002;35:L77.

47. Hyer MW. Stress Analysis of Fiber-reinforced Composite Materials. DEStech Publications, Inc; 2009. 718 p.

48. Product Detail [Internet]. [cited 2017 Nov 15]. Available from: http://www.epotek.com/site/component/products/productdetail.html?cid[0]=19

49. Ceramic Materials (PZT) - Boston Piezo-Optics Inc. [Internet]. [cited 2017 Dec 5]. Available from: http://www.bostonpiezooptics.com/ceramic-materials-pzt

Appendices

Appendix A

The following is the SAS code written and developed to determine significance of the fracture toughness data using a one-way ANOVA, as well as, pairwise comparisons between each of the different specimen type.

```
libname mydata 'V:\Spine Research\MTS Analysis\Spine Lab Data\Fracture
Toughness';

/* creating dataset named 'fracture_toughness' */
/*tell SAS that you want to input 'sampletype' as a categorical variable and
'fracturetoughness' as a continuous numeric response*/
/*start entering data*/

data fracture_toughness;
input sampletype $ fracturetoughness;
datalines;
Control 4.05
Control 2.52
Control 3.57
Control 3.01
Control 3.59
BS 3.06
BS 3.36
BS 1.86
BS 3.41
BS 1.88
TS 1.63
TS 1.94
TS 1.79
TS 2.79
TS 1.75

;
run;
/*End data entry*/

/*check the contents of this data set, ensure that fracturetoughness is a
continuous variable and sampletype is a categorical variable*/

proc contents data = fracture_toughness;
run;
ODS RTF FILE = 'V:\Spine Research\MTS Analysis\Spine Lab Data\Fracture
Toughness\ft_statsassumptions.RTF'; /*make file to save results*/
/* Create new dataset with a transformed response using the appropriate
formula */
data fracture_toughness;
set fracture_toughness;
```

```
ft_transform = 1/(fracturetoughness**0.5);
run;

proc print data=fracture_toughness;
run;


/* Run the ANOVA model using PROC GLM (General Linear Model) */

/* The SAS procedure GLM is called, the dataset name is 吐racture_toughness・
*/
/* This step declares 壮ampletype・as a categorical variable・*/
/* On the LHS of the model is the continuous response fracturetoughness, on
the RHS is the predictor sampletype */
/* Run the model */

proc glm data = fracture_toughness;
class sampletype;
model fracturetoughness = sampletype;
means unit/hovtest = bf;            /*Brown-Forsythe test for checking the
homogeneity*/
output out = checkfit predicted = y_hat residual = e_ij;
run;

/*normality plot of residuals*/
proc univariate data = checkFit normal plot;
var e_ij;
run;

/*residuals vs. predicted plot*/
proc sgplot data=checkfit;
scatter y = e_ij x = y_hat;
run;

ODS RTF Close;
quit;

ODS RTF FILE= 'V:\Spine Research\MTS Analysis\Spine Lab Data\Fracture
Toughness\ft_statstukey.RTF';
/* First run the ANOVA model, then check the validity of the statistical
assumptions. Then, conduct the multiple testing procedures*/
/* Code for different multiple testing procedures is given below */


proc glm data = fracture_toughness;
class sampletype;
model fracturetoughness = sampletype;
lsmeans sampletype/ pdiff=all adjust=tukey;     /*Tukey method*/
run;

ODS RTF CLOSE;
quit;
```

Appendix B

Screen shot of raw data collected for a 0.0 mm tensile testing specimen, for load (_load) vs the displacement measured (Laser Extensometer), revealing the lack of change in the extension measured. It is evident that the extension repeats itself with each point collected. The laser extensometer values are also not accurate to the decimal place shown because it can only capture with accuracy to the 1000th's place.

_Extension	_Load	Laser Extensometer
in	lbf	in
2.11E-05	0.999959173	0.147199997
4.69E-05	0.939127409	0.147199997
8.44E-05	1.028062971	0.147199997
1.24E-04	1.169354209	0.147199997
1.59E-04	1.308149145	0.147199997
1.92E-04	1.365520367	0.147199997
0.000225103	1.532057738	0.147199997
0.000257931	1.6075245	0.147199997
0.000290759	1.439110534	0.147199997
0.000321241	1.634865911	0.147199997
0.000351724	1.786837212	0.147199997
0.000382207	1.799381864	0.147199997
0.000415034	1.987064538	0.147199997
0.000447862	2.002994693	0.147199997
0.000483034	2.155240312	0.147199997
0.000515862	2.277146748	0.147199997
0.000551034	2.316568754	0.147199997
0.000581517	2.370956784	0.147199997
0.000614345	2.328953897	0.147199997

Appendix C

Theoretical transverse stiffness calculations of tensile samples 0.0 mm and 0.4 mm using The Rule of Mixtures for Composite Materials. Fiber volume and matrix volume ($V_{f0.4}$, $V_{m0.4}$) were calculated for the 0.4 mm type specimen. The fiber volume of the material was then calculated (V_f). Using an approximated stiffness of the PZT (E_f = 78000 MPa[49]) and a known stiffness of the epoxy matrix from Epotek (E_m = 2260 MPa) these were input into the Rule of Mixtures Equation for Composite Materials in the transverse direction, along with fiber volume.

$$V_{f0.4} = \pi r^2 \text{h}$$
$$= \pi(\frac{10\ mm}{2})^2\ (2.0\ \text{mm})$$
$$= 157.08\ mm^3$$

$$V_{m0.4} = l \times w \times h$$
$$= 11\ mm \times 11\ mm \times 1.6\ mm$$
$$= 193.6\ mm^3$$

$$V_f = \frac{V_{f0.4}}{V_{m0.4}} \times 100$$
$$= 36.\ 1\ \%$$

$$E_{2,0.4mm} = \frac{E_f E_m}{E_m V_f + E_f(1 - V_f)}$$

$$= \frac{(78000\ MPa)(2260\ MPa)}{(2260\ MPa)(0.361) + 78000MPa(1 - 0.361)}$$

$$\approx 3480\ MPa \text{ for the 0.4 mm specimen}$$

$$E_{2,0.0mm} = \frac{E_f E_m}{E_m V_f + E_f(1 - V_f)}$$

$$= \frac{(78000\ MPa)(2260\ MPa)}{(2260\ MPa)(1) + 78000MPa(1 - 1)}$$

$$\approx 78{,}000\ MPa \text{ for the 0.0 mm specimen}$$